Annular PIP_3 accumulation controls actin architecture and modulates cytotoxicity at the immunological synapse

Audrey Le Floc'h,[1] Yoshihiko Tanaka,[3] Niels S. Bantilan,[1] Guillaume Voisinne,[2] Grégoire Altan-Bonnet,[2] Yoshinori Fukui,[3] and Morgan Huse[1]

[1]Immunology Program, [2]Computational Biology Program, Memorial Sloan-Kettering Cancer Center, New York, NY 10065
[3]Division of Immunogenetics, Department of Immunobiology and Neuroscience, Medical Institute of Bioregulation, Kyushu University, Fukuoka 812-8582, Japan

The immunological synapse formed by a T lymphocyte on the surface of a target cell contains a peripheral ring of filamentous actin (F-actin) that promotes adhesion and facilitates the directional secretion of cytokines and cytolytic factors. We show that growth and maintenance of this F-actin ring is dictated by the annular accumulation of phosphatidylinositol trisphosphate (PIP_3) in the synaptic membrane. PIP_3 functions in this context by recruiting the exchange factor Dock2 to the periphery of the synapse, where it drives actin polymerization through the Rho-family GTPase Rac. We also show that synaptic PIP_3 is generated by class IA phosphoinositide 3-kinases that associate with T cell receptor microclusters and are activated by the GTPase Ras. Perturbations that inhibit or promote PIP_3-dependent F-actin remodeling dramatically affect T cell cytotoxicity, demonstrating the functional importance of this pathway. These results reveal how T cells use lipid-based signaling to control synaptic architecture and modulate effector responses.

CORRESPONDENCE
Morgan Huse:
husem@mskcc.org

Abbreviations used: GEF, guanine nucleotide exchange factor; GST, glutathione S-transferase; IS, immunological synapse; MTOC, microtubule-organizing center; PBD, p21-binding domain; PDMS, polydimethylsiloxane; PI, propidium iodide; PI3K, phosphoinositide 3-kinase; PIP_3, phosphatidylinositol 3,4,5-trisphosphate; TIRF, total internal reflection fluorescence.

Stimulation of the TCR induces dramatic cytoskeletal remodeling that reshapes the interface between the T cell and the APC into an immunological synapse (IS; Gomez and Billadeau, 2008; Dustin et al., 2010). First, an intense burst of actin polymerization drives radially symmetric spreading over the APC. Subsequently, the filamentous actin (F-actin) within this circular lamellipodium resolves into an annular configuration (Bunnell et al., 2001; Stinchcombe et al., 2006; Sims et al., 2007). The resulting F-actin ring regulates the trafficking and clustering of signaling complexes and integrins (Varma et al., 2006; Nguyen et al., 2008; Babich et al., 2012; Yi et al., 2012). It also provides a structural framework for specifying effector function. Clearance of F-actin from the central synaptic membrane is coupled to the polarization of the microtubule-organizing center (MTOC) toward the APC (Huse, 2012). These events together facilitate the directional release of soluble factors into the IS. This is particularly important for $CD8^+$ CTLs, which kill APCs by directional secretion of cytolytic perforins and granzymes (Stinchcombe and Griffiths, 2007).

The pathways regulating synaptic F-actin architecture are not well understood. Studies suggest that TCR-induced actin polymerization and cell spreading require the Rho family GTPase Rac (Ku et al., 2001; Sanui et al., 2003; Nolz et al., 2006; Zipfel et al., 2006). Like all small GTPases, Rac is activated by specific guanine nucleotide exchange factors (GEFs) that catalyze its transition from an inactive, GDP-bound form into an active, GTP-bound form that recruits downstream effectors (Jaffe and Hall, 2005). T cells express several GEFs that could potentially regulate Rac. The most prominent is Vav, which functions as a core component of the TCR signaling complex (Tybulewicz, 2005). Recent work, however, has suggested that GEFs other than Vav might control Rac-dependent F-actin remodeling at the IS (Miletic et al., 2009). T cells also express Dock2, a Rac-specific CDM family GEF that catalyzes nucleotide exchange via its conserved DHR-2 domain (Côté and Vuori, 2007). T cells lacking Dock2 display marked defects in Rac activation and TCR trafficking (Sanui et al., 2003), implying that Dock2 might be involved

The Rockefeller University Press $30.00
J. Exp. Med. 2013 Vol. 210 No. 12 2721-2737
www.jem.org/cgi/doi/10.1084/jem.20131324

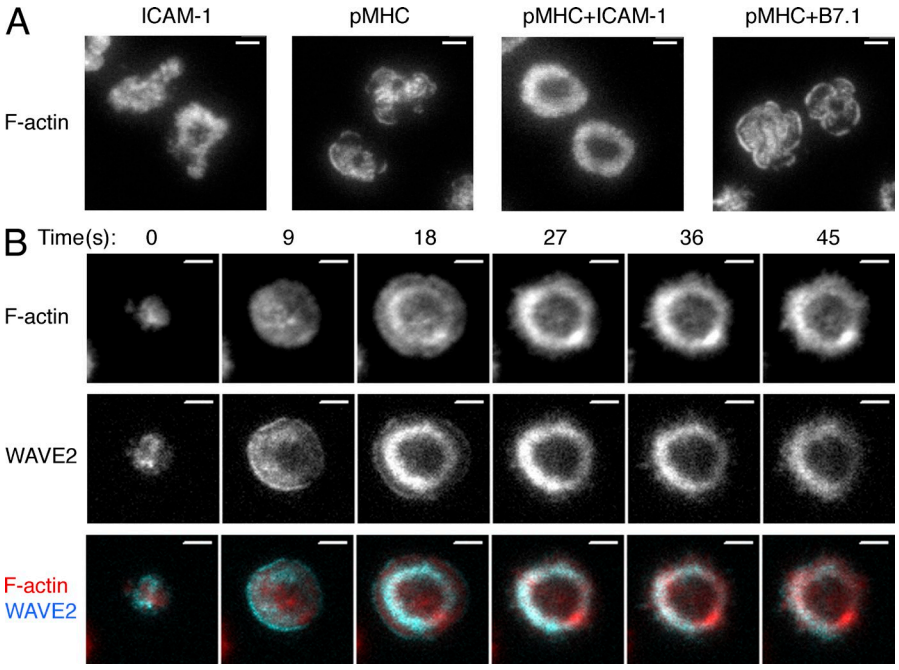

Figure 1. T cells form stable F-actin rings on bilayers containing pMHC and ICAM-1. (A) OT-1 CTLs were stimulated for 10 min on bilayers containing the indicated ligands, fixed, and stained with fluorescently labeled phalloidin. Representative TIRF images are shown. Images are representative of at least 100 cells imaged over at least two independent experiments. (B) OT-1 CTLs expressing RFP-labeled Lifeact together with GFP-labeled WAVE2 were analyzed by TIRF microscopy on bilayers containing pMHC and ICAM-1. A representative time-lapse montage (9-s intervals) is shown. Images are representative of at least 150 cells imaged over four independent experiments. Bars, 5 µm.

in shaping synaptic F-actin. The N-terminal region of Dock2 binds constitutively to the scaffolding protein Elmo, which confers stabilization and enhances GEF activity toward Rac. Dock2 also contains a so-called DHR-1 domain, which binds specifically to phosphatidylinositol 3,4,5-trisphosphate (PIP_3; Côté and Vuori, 2007). In that regard, it is intriguing that TCR signaling induces robust PIP_3 accumulation at the IS (Costello et al., 2002; Harriague and Bismuth, 2002; Huppa et al., 2003; Garçon et al., 2008). The possibility that this pool of PIP_3 might regulate F-actin organization via recruitment of Dock2, however, has not been explored.

It is generally thought that synaptic PIP_3 is produced by class I phosphoinositide 3-kinases (PI3Ks). It remains controversial, however, precisely which isoforms contribute to this process (Alcázar et al., 2007; Garçon et al., 2008; Sauer et al., 2008), and it is also unclear how these proteins might be recruited and activated by TCR signaling. Previous studies in T cells have focused on the role of phosphotyrosine (pTyr)-containing signaling motifs that can bind and allosterically activate certain PI3K isoforms (Carpenter et al., 1993; Holt et al., 1994; Pagès et al., 1994; Zhang et al., 1998; Shim et al., 2004, 2011). However, class I PI3Ks also interact with the small GTPase Ras (Rodriguez-Viciana et al., 1994, 1996), which functions synergistically with pTyr peptides to induce full PI3K activity (Jimenez et al., 2002). Ras is strongly activated by TCR signaling (Genot and Cantrell, 2000), but whether it promotes synaptic PIP_3 accumulation through PI3K is not known.

In the present study, we demonstrate that the size and shape of the synaptic F-actin ring is dictated by an annular accumulation of PIP_3 in the overlying plasma membrane. This PIP_3 is generated by class IA PI3K isoforms downstream of Ras, and coordinates F-actin architecture by recruiting the Dock2/Elmo complex to the periphery of the IS. Specific perturbations in PIP_3–Dock2 signaling either reduce or enhance CTL-mediated killing, indicative of an important role in T cell effector responses. These results identify a previously uncharacterized mechanism for controlling synaptic F-actin, and provide insight into how lipid second messenger signaling shapes lymphocyte structure and function.

RESULTS

Synaptic growth and F-actin ring formation require Rac

To study F-actin architecture at the IS, we used total internal reflection fluorescence (TIRF) microscopy to image OT-1 CTLs on supported lipid bilayers containing H-$2K^b$ bound to the ovalbumin$_{257-264}$ peptide, the cognate peptide MHC (pMHC) for the OT-1 TCR. We also included the adhesion molecule ICAM-1, which is recognized by the $\alpha_L\beta_2$ integrin LFA-1. Consistent with previous work (Sims et al., 2007; Beemiller et al., 2012), CTLs formed stable, radially symmetric contacts on these surfaces characterized by peripheral F-actin rings (Fig. 1 A). Bilayers containing pMHC or ICAM-1 alone did not elicit robust ring formation, nor did bilayers containing pMHC and B7.1, a ligand for the costimulatory receptor CD28 (Acuto and Michel, 2003; Fig. 1 A). Hence, simultaneous engagement of the TCR and LFA-1 was required for stable F-actin ring formation. This observation is consistent with previous studies demonstrating the importance of combined stimulation through LFA-1 and an activating receptor for establishing radially symmetric organization within the IS (Somersalo et al., 2004; Anikeeva et al., 2005; Markiewicz et al., 2005).

Live imaging experiments revealed that F-actin progressed through two distinct architectural phases during IS formation (Fig. 1 B and Video 1). Contact with the bilayer initially induced rapid cell spreading, accompanied by a relatively featureless distribution of F-actin beneath the plasma membrane. Within

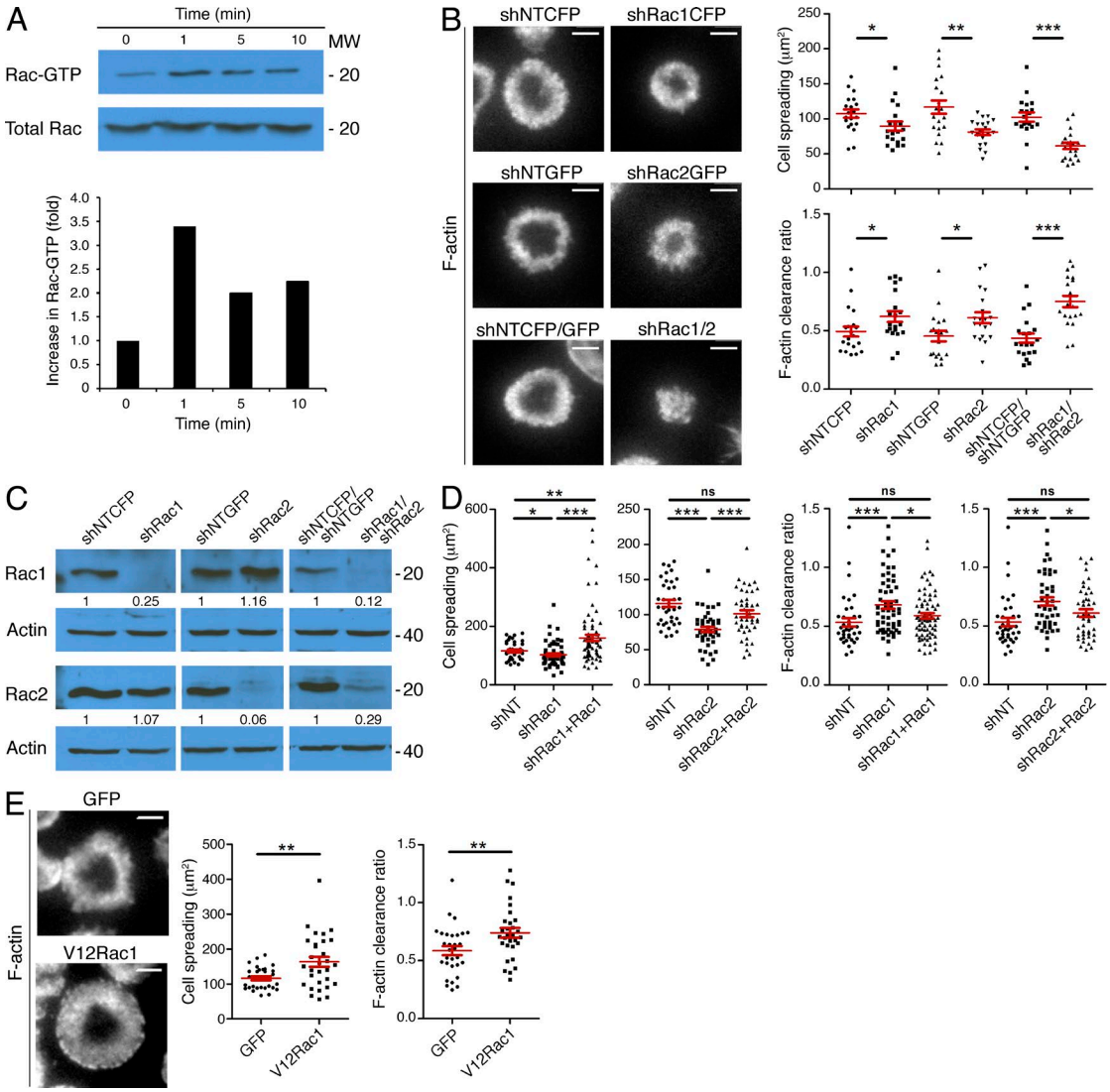

Figure 2. Rac1 and Rac2 are essential for synaptic F-actin remodeling. (A) OT-1 CTLs were stimulated for the indicated times with beads coated with pMHC and ICAM-1. Top, active Rac was isolated using GST-PAK1-PBD and visualized by immunoblot. Bottom, quantification of activated Rac from the blot shown above, corrected using total Rac expression and normalized to the first time point. (B) OT-1 CTLs were transduced with nontargeting control shRNA (shNT) or shRNA specific for Rac1 and/or Rac2. Cells were then stimulated on lipid bilayers containing pMHC and ICAM-1, fixed, and stained with fluorescently labeled phalloidin. Representative TIRF images are shown (left). Cell spreading (top graph) and F-actin clearance ratio (bottom graph) were quantified for each condition (n = 20 cells). (C) shRNA-transduced OT-1 CTLs were probed for Rac1 and Rac2 by immunoblot. Numbers denote corrected, normalized amounts of Rac1 and Rac2 in each lane (see Materials and methods). (D) OT-1 CTLs were transduced with the indicated shRNAs together with shRNA-resistant, GFP-labeled Rac1 or Rac2 as shown. Transduced cells were stimulated as described in B, and F-actin was visualized by phalloidin staining. Quantification of cell spreading and F-actin clearance ratio is shown ($n \geq 37$ cells). (E) OT-1 CTLs expressing GFP-labeled V12Rac1 or GFP alone were stimulated as described in B, and F-actin was analyzed by phalloidin staining. Representative TIRF images are shown (left). Right, quantification of cell spreading and F-actin clearance ratio (n = 30 cells). Bars, 5 µm. In scatter plots, red lines and error bars denote the mean and SEM, respectively. P-values were calculated using the Mann-Whitney test (two-tailed). ***, $P < 0.001$, **, $P < 0.01$, *, $P \leq 0.05$, and ns, $P > 0.05$. All data are representative of at least two independent experiments.

20 s, IS growth stopped and the F-actin distribution resolved into an intense ring. The Rac effector WAVE2, which drives actin polymerization through the Arp2/3 complex, accumulated in an annular configuration before reorganization of F-actin into a ring, and it remained colocalized with F-actin as the IS matured. This result suggested that activated Rac is involved in both the expansion and consolidation phases of IS formation.

To determine if the kinetics of Rac activation is consistent with this role, we quantified GTP-Rac levels by pulldown assay using the p21-binding domain (PBD) of PAK. Co-engagement of the TCR and LFA-1 induced robust Rac activation in CTLs within 1 min that was sustained for at least 10 min after that (Fig. 2 A). This profile correlates well with IS formation, which occurs over a similar timescale.

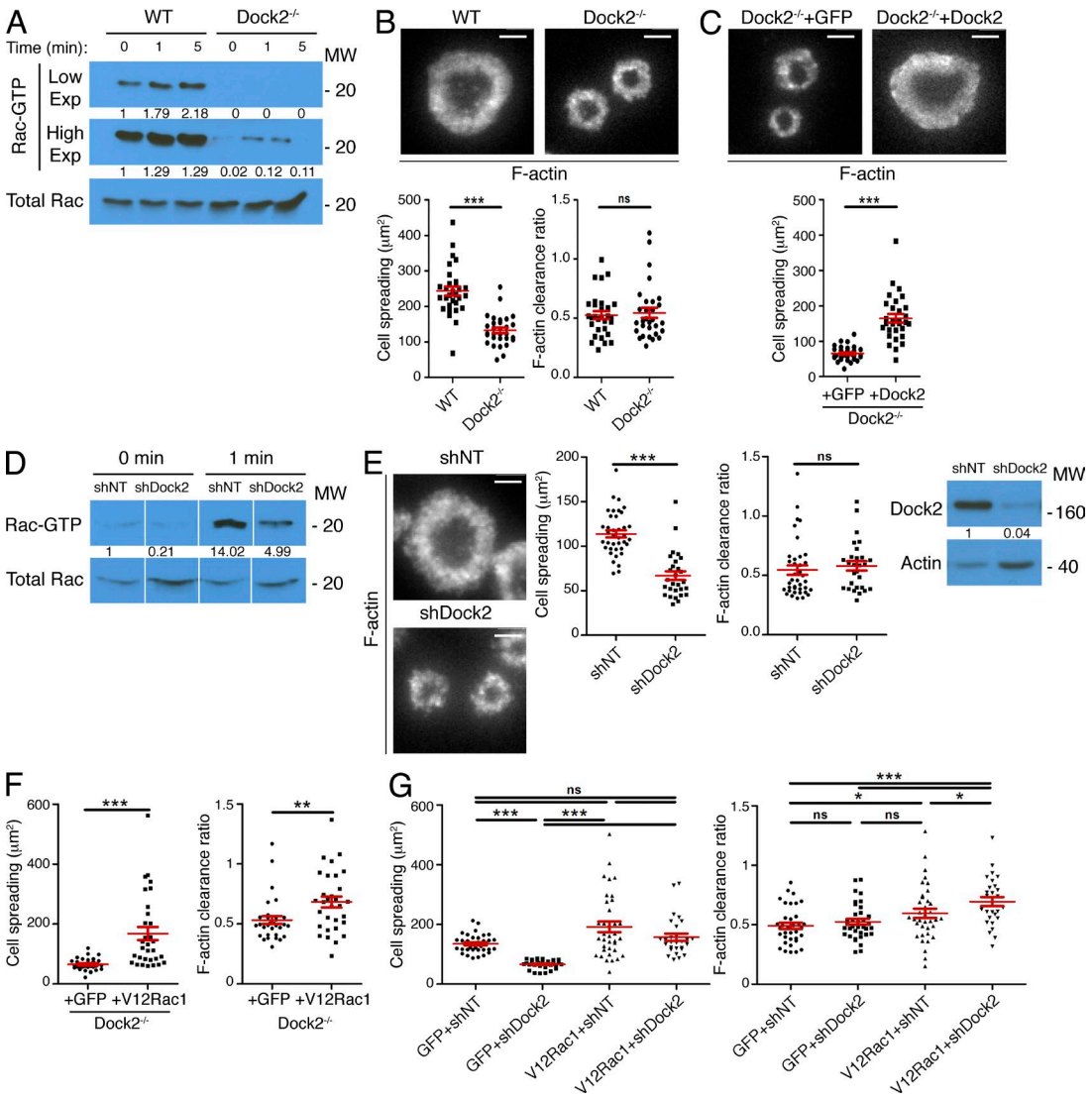

Figure 3. Dock2 drives F-actin dynamics at the IS through Rac. (A) 2B4 T cell blasts from Dock2$^{+/+}$ (WT) and Dock2$^{-/-}$ mice were stimulated for the indicated times with beads coated with pMHC and ICAM-1. Cell extracts were incubated with GST-PAK1-PBD, and activation of Rac analyzed by immunoblot. Numbers denote corrected, normalized amounts of activated Rac in each lane, quantified from high and low film exposures, as indicated. (B) WT and Dock2$^{-/-}$ 2B4 T cells were stimulated on bilayers containing pMHC and ICAM-1, fixed, and stained with fluorescently labeled phalloidin. Representative TIRF images are shown (top). Bottom, quantification of cell spreading and F-actin clearance ratio (n = 30 cells). (C) Dock2$^{-/-}$ 2B4 T cells expressing GFP-labeled Dock2 or GFP alone were stained with phalloidin after spreading on stimulatory bilayers. Representative TIRF images are shown (top). Bottom, quantification of cell spreading ($n \geq 30$ cells). (D and E) OT-1 CTLs were transduced with nontargeting control shRNA (shNT) or shRNA specific for Dock2. (D) Transduced cells were stimulated with beads coated with pMHC and ICAM-1, and Rac activation was analyzed by pulldown assay using GST-PAK1-PBD. Numbers denote corrected, normalized amounts of activated Rac. (E) Transduced cells were stimulated on lipid bilayers containing pMHC and ICAM-1, fixed, and stained with fluorescently labeled phalloidin. Representative TIRF images are shown (left). Middle, quantification of cell spreading and F-actin clearance ratio ($n \geq 30$ cells). Right, transduced cells were probed for Dock2 by immunoblot. Numbers denote corrected, normalized amounts of Dock2. (F and G) Dock2-deficient 2B4 T cells (F) and shDock2-expressing OT-1 CTLs (G) were transduced with GFP-labeled V12Rac1 or GFP alone, stimulated as described in B, and imaged after phalloidin staining. Quantification of cell spreading and F-actin clearance ratio are shown ($n > 30$ cells for Dock2$^{-/-}$ experiment; $n \geq 28$ cells for shDock2 experiment). Bars, 5 µm. In scatter plots, red lines and error bars denote the mean and SEM, respectively. P-values were calculated using the Mann-Whitney test. ***, $P < 0.001$, **, $P < 0.01$, *, $P \leq 0.05$, and ns, $P > 0.05$. All data are representative of at least two independent experiments.

To determine whether Rac activity is necessary for IS growth and organization, we used shRNA transduction to suppress Rac1 and Rac2, the two Rac isoforms expressed in T cells. Relative to control cells expressing nontargeting shRNA, OT-1 CTLs lacking Rac1 or Rac2 exhibited significantly reduced cell spreading on bilayers containing pMHC and ICAM-1 (Fig. 2, B and C). Simultaneous suppression of both Rac isoforms led to an even greater reduction in IS size, implying that the proteins function additively in this context. Rac-deficient CTLs also displayed defects in F-actin ring formation

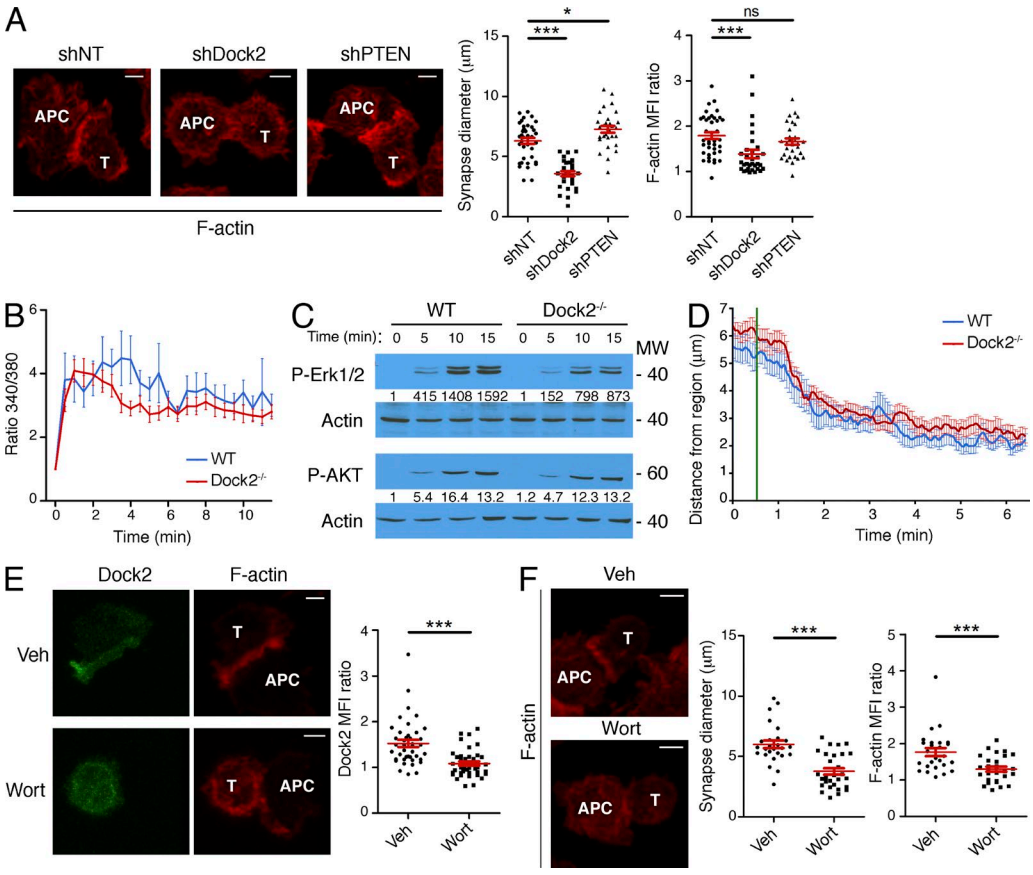

Figure 4. PIP_3–Dock2 signaling is required for F-actin accumulation in CTL–target cell conjugates. (A) OT-1 CTLs expressing nontargeting (NT) control shRNA or shRNA against Dock2 or PTEN were mixed with OVA-pulsed RMA-s cells and the conjugates imaged by confocal microscopy after fixation and staining with fluorescently labeled phalloidin. Representative images are shown on the left. Right, quantification of IS size and synaptic F-actin enrichment (see Materials and methods). (B) Fura-2AM–loaded WT and Dock2$^{-/-}$ 2B4 T cells were imaged on lipid bilayers containing pMHC and ICAM-1. Mean, background-corrected Fura-2AM ratios are plotted versus time for each condition (n = 12 cells). (C) Immunoblot analysis of phospho-Erk1/2 (P-Erk1/2) and phospho-AKT (P-AKT) in WT and Dock2$^{-/-}$ 2B4 T cells stimulated on lipid bilayers for the indicated times. Numbers denote corrected, normalized amounts of P-Erk1/2 and P-AKT. (D) WT and Dock2$^{-/-}$ 2B4 T cells expressing GFP-labeled tubulin were attached to glass surfaces containing immobilized, photoactivatable pMHC. Localized UV irradiation was then used to activate TCRs in a small region of membrane, and the position of the MTOC monitored by epifluorescence microscopy. The mean distance between the MTOC and the irradiated region is plotted against time (n > 20 cells), with UV irradiation indicated by the green line. Error bars denote SEM. (E) Left, representative images of phalloidin-stained conjugates formed by OVA-pulsed RMA-s cells and OT-1 CTLs expressing GFP-labeled Dock2 either in the presence of wortmannin or vehicle control (Veh). Right, quantification of synaptic Dock2 enrichment. (F) Left, representative images of phalloidin-stained conjugates formed by OVA-pulsed RMA-s cells and OT-1 CTLs in the presence of wortmannin (Wort) or vehicle control (Veh). Right, quantification of IS size and synaptic F-actin enrichment. In all images, T cells and APCs are indicated with white text. Bars, 3 µm. In scatter plots, red lines and error bars denote the mean and SEM, respectively. P-values were calculated using the Mann-Whitney test. ***, P < 0.001, *, P ≤ 0.05, and ns, P > 0.05. Data in A, E, and F were pooled from two independent experiments. Data in B–D are representative of at least two independent experiments.

(Fig. 2 B), which we quantified using a "clearance ratio" parameter for each cell that compares the fluorescence intensity at the edge of the IS with that of the center. We expect a clearance ratio of ∼1 for uniform fluorescence distributions and <1 for annular patterns (see Materials and methods). Importantly, expression of shRNA-resistant forms of Rac1 and Rac2 in CTLs lacking either GTPase reversed defects in both cell spreading and F-actin organization, indicating that the observed phenotypes were specific (Fig. 2 D). We also analyzed OT-1 CTLs expressing a constitutively active Rac1 mutant (V12Rac1). On stimulatory bilayers, these cells exhibited a substantial increase in synaptic size relative to controls expressing GFP alone (Fig. 2 E). This enhanced cell spreading was accompanied by reduced F-actin clearance at the center of the IS, consistent with V12Rac1 inducing unregulated actin polymerization. Collectively, these data indicate that Rac activity plays a key role in synaptic F-actin remodeling.

Dock2/Elmo modulates Rac and F-actin at the IS

Next, we investigated whether the Dock2/Elmo complex is required for growth and stabilization of synaptic F-actin. For these experiments, we used CD4$^+$ Dock2$^{-/-}$ T cells expressing the 2B4 TCR, which recognizes the moth cytochrome $c_{88\text{-}103}$ peptide bound to I-E^k. Consistent with previous work (Sanui et al., 2003), we found that basal and TCR-induced Rac activation was strikingly diminished in T cells lacking

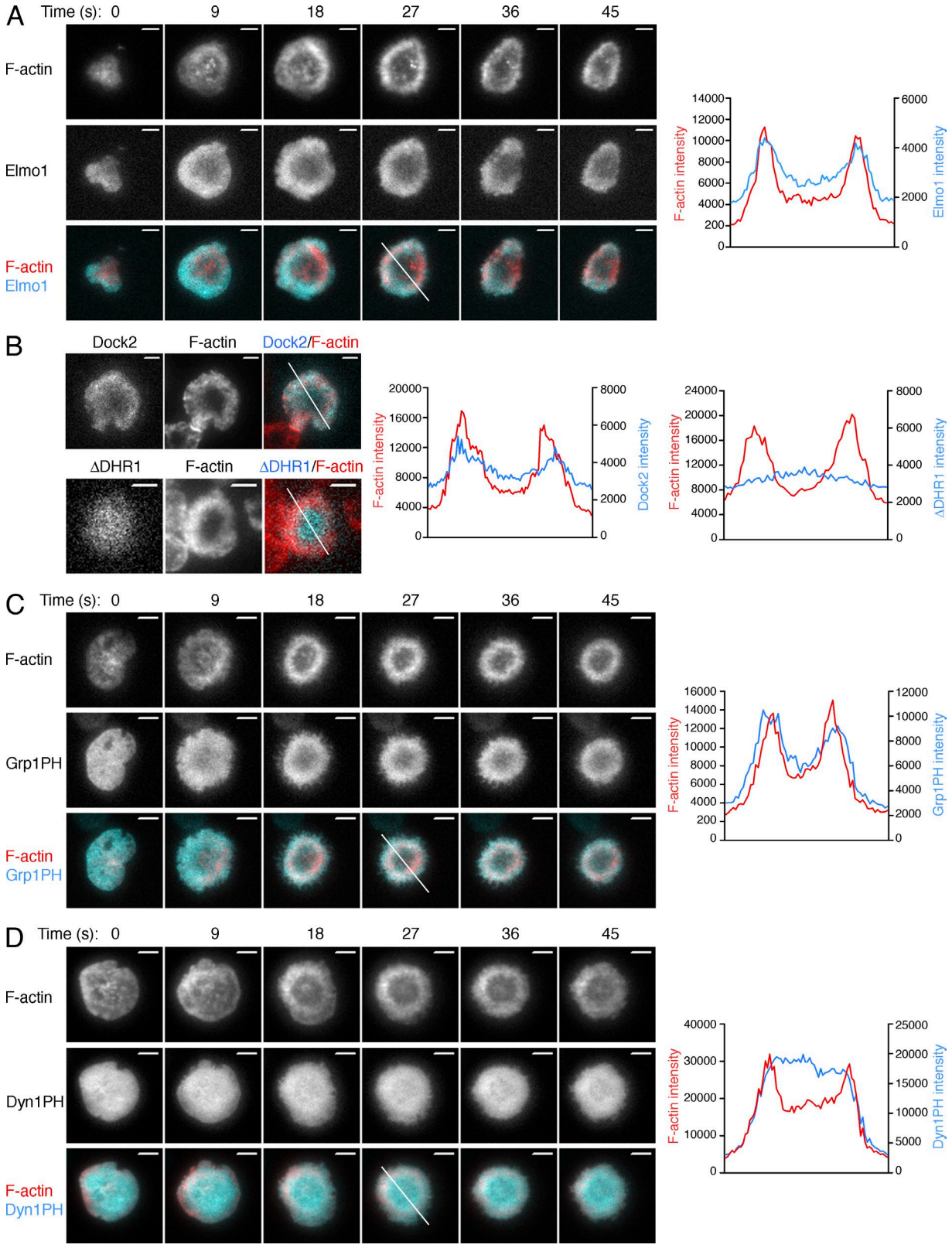

Figure 5. Dock2/Elmo and PIP_3 localization at the IS. (A) OT-1 CTLs expressing RFP-labeled Lifeact together with GFP-labeled Elmo1 were analyzed by TIRF microscopy on lipid bilayers containing pMHC and ICAM-1. Left, representative time-lapse montages (9-s intervals). Right, linescans (derived from the white line in the left panel, time = 27 s) showing F-actin and Elmo1 accumulation. (B) OT-1 CTLs expressing GFP-fusions of either Dock2 or a Dock2 mutant lacking the DHR-1 domain (ΔDHR1) were imaged on stimulatory bilayers after fixation and staining with phalloidin. Left, representative TIRF

Dock2 (Fig. 3 A). These cells displayed a dramatic spreading defect, forming miniaturized synapses on stimulatory bilayers (Fig. 3 B). Interestingly, we did not observe a significant defect in IS organization; the F-actin rings that formed were simply smaller and less substantial (Fig. 3 B). Expression of full length Dock2 in Dock2$^{-/-}$ T cells reversed this phenotype, indicating that it resulted specifically from Dock2 deficiency (Fig. 3 C). We also analyzed OT-1 CTLs expressing shRNA against Dock2, which displayed defects similar to those observed in Dock2$^{-/-}$ 2B4 T cells (Fig. 3, D and E). Notably, suppression or deletion of Dock2 did not reverse the impaired F-actin ring formation and exuberant IS growth induced by V12Rac1 (Fig. 3, F and G). Hence, Dock2/Elmo operates upstream of Rac to promote IS growth in both CD4$^+$ and CD8$^+$ T cells.

To determine whether Dock2 also controls F-actin accumulation during IS formation with APCs, we analyzed fixed conjugates composed of OT-1 CTLs and antigen-loaded RMA-s cells. F-actin is known to accumulate at the CTL–target cell interface within minutes of TCR stimulation (Dustin and Long, 2010). Suppression of Dock2 abolished this enrichment of F-actin and significantly reduced IS size (Fig. 4 A). These data further support the idea that Dock2 is crucial for synaptic actin polymerization.

TCR-induced Ca^{2+} flux was normal in the absence of Dock2 (Fig. 4 B), indicating that early TCR signaling was largely intact. The PI3K pathway, which we assessed by phosphorylation of the PIP_3-dependent kinase AKT, was also unaffected (Fig. 4 C). Dock2 deficiency did lead to a slight decrease in Erk1/2 phosphorylation (Fig. 4 C), as reported previously (Sanui et al., 2003). However, we have found that Erk signaling is not required for IS growth and F-actin ring formation (see Fig. 10), implying that Erk1/2 phosphorylation is either independent of or downstream of Dock2-mediated F-actin growth. We also examined TCR-induced reorientation of the MTOC using an established photoactivation approach (Quann et al., 2009). This response was unaffected in Dock2$^{-/-}$ T cells (Fig. 4 D), indicating that Dock2 does not influence TCR-induced remodeling of the microtubule cytoskeleton.

Next, we examined whether the localization of the Dock2/Elmo complex is consistent with a role in the regulation of synaptic F-actin. Live imaging studies of OT-1 CTLs expressing GFP-labeled Elmo1 together with Lifeact-RFP revealed a close correspondence between the two fluorescent probes during both cell spreading and peripheral F-actin ring formation (Fig. 5 A and Video 2). F-actin also colocalized with Dock2-GFP (Fig. 5 B), implying that the pattern displayed by GFP-Elmo1 accurately reflected the behavior of the intact complex. Collectively with the results described above, these imaging data indicate a specific role for Dock2/Elmo in promoting F-actin growth at the IS.

Annular PIP_3 accumulation controls synaptic F-actin architecture

To explore the relationship between PIP_3 and F-actin in our system, we imaged OT-1 CTLs expressing Lifeact-RFP together with a PIP_3 biosensor containing GFP fused to the pleckstrin homology (PH) domain of Grp1 (Kavran et al., 1998). Strikingly, PIP_3 adopted an annular accumulation pattern at the IS concomitant with formation of the F-actin ring (Fig. 5 C and Video 3). Importantly, the PH domain of dynamin, which does not recognize PIP_3, distributed evenly over the surface of the IS at all time points (Fig. 5 D and Video 4). Hence, the annular pattern observed for the Grp1 PH domain resulted from its PIP_3 binding function.

The similarity between the Elmo1 and Grp1 PH accumulation patterns suggested that PIP_3 might be controlling Dock2/Elmo localization at the IS. Consistent with this hypothesis, treatment with the PI3K inhibitor wortmannin blocked annular accumulation of Elmo1 (Fig. 6 A). Wortmannin also blocked synaptic enrichment of GFP-labeled Dock2 in CTL–target cell conjugates (Fig. 4 E). TCR-induced Ca^{2+} flux was normal in wortmannin-treated cells (Fig. 6 B), suggesting that the impaired recruitment of Dock2/Elmo we observed did not result from a reduction in TCR signaling. Because the DHR-1 domain of Dock2 is known to bind PIP_3, we compared the localization of wild-type Dock2 with a Dock2 mutant lacking the DHR-1 domain (Dock2-ΔDHR1). Whereas wild-type Dock2 adopted an annular accumulation pattern, Dock2-ΔDHR1 exhibited a uniform distribution (Fig. 5 B). Together, these data indicated that PIP_3 operates upstream of Dock2/Elmo at the IS. Consistent with this interpretation, we found that PIP_3 accumulation was unaffected in Dock2$^{-/-}$ T cells (Fig. 6 C).

One would expect that perturbations disrupting Dock2/Elmo localization would affect synaptic F-actin remodeling. Indeed, wortmannin treatment inhibited cell spreading on stimulatory bilayers and significantly reduced IS size and synaptic F-actin enrichment in CTL–target cell conjugates (Fig. 6 D and Fig. 4 F). Wortmannin also inhibited TCR-induced Rac activation (Fig. 6 E), indicating that PIP_3 functions upstream of Rac in this system. Consistent with this interpretation, expression of V12Rac1 reversed the cell spreading phenotype induced by wortmannin (Fig. 6 F). Inhibition of PI3K also led to a substantial defect in F-actin ring formation (Fig. 6 D). These data strongly suggest that PIP_3 controls both growth and organization of synaptic F-actin.

PI3K function is antagonized by the 3′ phosphoinositide phosphatase PTEN (Buckler et al., 2008). To further explore the role of PIP_3 in IS architecture, we used shRNA against PTEN to enhance PI3K signaling. Basal and TCR-induced

images are shown. Right, linescans (derived from the white lines in the images to the left) showing F-actin and Dock2 accumulation at the IS. (C and D) OT-1 CTLs expressing RFP-labeled Lifeact together with GFP-labeled Grp1PH (C) or DynPH (D) were analyzed by TIRF microscopy on lipid bilayers containing pMHC and ICAM-1. Left, representative time-lapse montages (9-s intervals). Right, linescans (derived from the white line in the left panel, time = 27 s) showing F-actin and Grp1PH/Dyn1PH accumulation. Bars, 5 µm. Images in A, C, and D are representative of at least 80 cells imaged over at least four independent experiments. Images in B are representative of at least 12 cells imaged over two independent experiments.

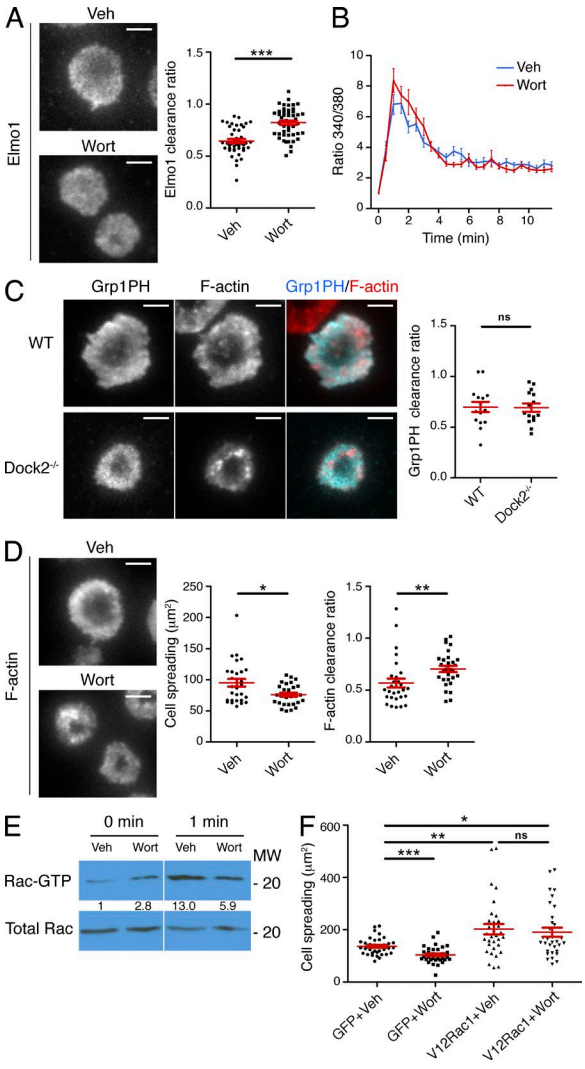

Figure 6. PIP_3 controls Rac-dependent F-actin dynamics through Dock2/Elmo. (A) OT-1 CTLs expressing GFP-labeled Elmo1 were pretreated with wortmannin (Wort) or vehicle control (Veh) and imaged on stimulatory lipid bilayers after fixation. Left, representative TIRF images are shown. Right, quantification of Elmo1 clearance ratio ($n > 40$ cells). (B) Fura-2AM–loaded OT-1 CTLs pretreated with wortmannin or vehicle were imaged on lipid bilayers containing pMHC and ICAM-1. Mean, background-corrected Fura-2AM ratios are plotted versus time for each condition ($n = 20$ cells). Error bars denote SEM. (C) WT and Dock2$^{-/-}$ 2B4 T cells expressing GFP-labeled Grp1PH were imaged on lipid bilayers containing pMHC and ICAM-1 after phalloidin staining. Left, representative TIRF images are shown. Right, quantification of Grp1PH clearance ratio ($n = 15$ cells). (D) OT-1 CTLs were treated with wortmannin as indicated, stimulated on bilayers containing pMHC and ICAM-1, and stained with fluorescently labeled phalloidin. Left, representative TIRF images are shown. Right, quantification of cell spreading and F-actin clearance ratio ($n \geq 30$ cells). (E) OT-1 CTLs pretreated with wortmannin as indicated were stimulated with beads coated with pMHC and ICAM-1. Cell extracts were incubated with GST-PAK1-PBD and activation of Rac was determined by immunoblot. Numbers denote corrected, normalized amounts of activated Rac. (F) CTLs expressing GFP-labeled V12Rac1 or GFP alone were treated with wortmannin as indicated and then stimulated and imaged as described in D. Quantification of cell spreading is shown ($n \geq 30$ cells). Bars, 5 µm. In scatter plots, red lines and error bars denote the mean and SEM, respectively. P-values were calculated using the Mann-Whitney test. ***, $P < 0.001$, **, $P < 0.01$, *, $P \leq 0.05$, and ns, $P > 0.05$. All data are representative of at least two independent experiments.

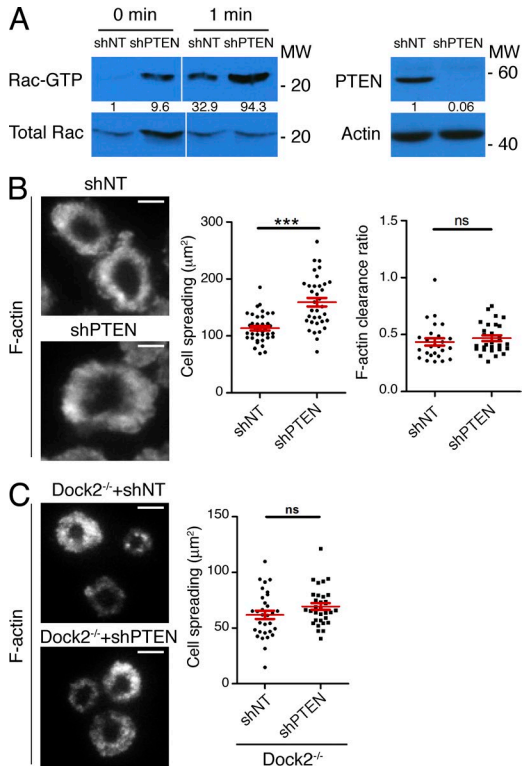

Figure 7. PTEN regulates Rac activation and IS growth. (A) Left, OT-1 CTLs expressing shRNA specific for PTEN or a control shRNA (shNT) were stimulated with beads coated with pMHC and ICAM-1. Cell extracts were incubated with GST-PAK1-PBD, and activation of Rac was determined by immunoblot. Numbers denote corrected, normalized amounts of activated Rac. Right, CTL lysates were probed for PTEN by immunoblot. Numbers denote corrected, normalized amounts of PTEN. (B) OT-1 CTLs expressing shRNA against PTEN or nontargeting control shRNA were imaged on stimulatory bilayers after phalloidin staining. Left, representative TIRF images are shown. Right, quantification of cell spreading and F-actin clearance ratio ($n = 35$ cells). (C) Dock2$^{-/-}$ 2B4 T cells expressing the indicated shRNAs were imaged on stimulatory bilayers as described in B. Left, representative TIRF images are shown. Right, quantification of cell spreading ($n > 30$ cells). Bars, 5 µm. In scatter plots, red lines and error bars denote the mean and SEM, respectively. P-values were calculated using the Mann-Whitney test. ***, $P < 0.001$ and ns, $P > 0.05$. Data are representative of at least two independent experiments.

Rac activation were both dramatically increased in CTLs lacking PTEN (Fig. 7 A). These cells also displayed a marked increase in IS size on stimulatory bilayers and in CTL–target cell conjugates (Fig. 7 B and Fig. 4 A). We observed a similar phenotype after deleting the PTEN gene in CTLs using the Cre-Lox system (unpublished data). Interestingly, F-actin ring formation was largely intact in the absence of PTEN (Fig. 7 B),

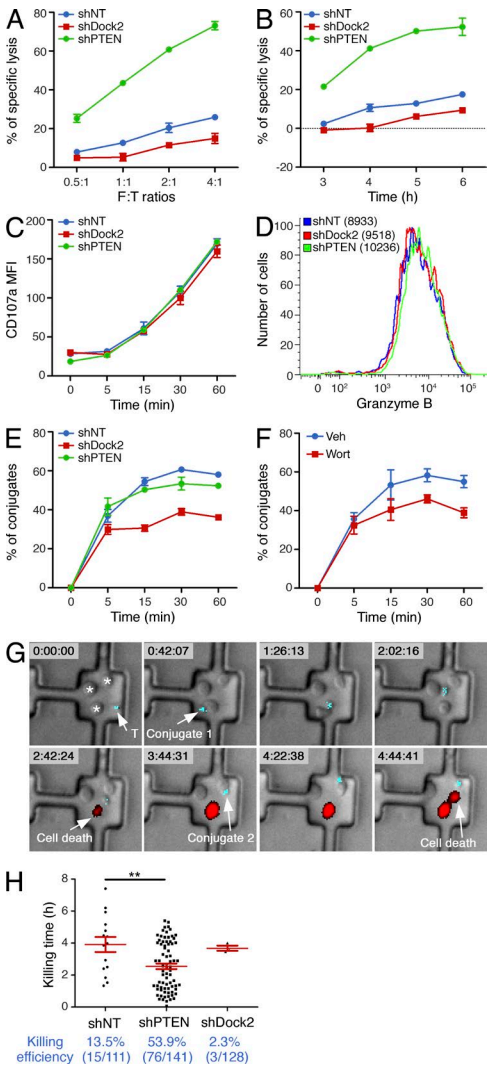

Figure 8. PI3K–Dock2 signaling modulates the efficiency of target cell killing. (A–C) RMA-s target cells loaded with 100 nM OVA peptide were mixed with OT-1 CTLs expressing either nontargeting shRNA or shRNA specific for Dock2 or PTEN. (A and B) Specific lysis of target cells at the indicated effector to target (E:T) ratios after 6 h (A), or at the indicated times at an E:T ratio of 2:1 (B). Killing assays were performed in triplicate. (C) Cell surface exposure of CD107a was determined by flow cytometry. (D) OT-1 CTLs expressing the indicated shRNA constructs were stained using antibodies against granzyme B and analyzed by flow cytometry. (E and F) RMA-s target cells loaded with 100 nM OVA peptide were mixed with shRNA-expressing (E) or wortmannin-treated (F) OT-1 CTLs as indicated. CTL–target cell conjugate formation was assessed by gating on the GFP$^+$ (CTLs), PKH26$^+$ (RMA-s targets) population (see Materials and methods). Degranulation and conjugate assays were performed in duplicate at an E:T ratio of 1:1. Error bars indicate SEM. (G and H) OT-1 CTLs and RMA-s targets were imaged in PDMS wells in the presence of PI to detect killing events. (G) Time-lapse montage showing the killing of two RMA-s cells by a CTL expressing shRNA against PTEN. Time is shown (hours:minutes:seconds) at the top of each image. White arrows indicate conjugate formation and killing events. (H) Top, quantification of killing time, with red lines and bars indicating mean and SEM, respectively. Bottom, killing efficiency of monogamous CTL–target cell contacts is shown in blue. In scatter plots, red lines and error bars denote the mean and SEM, respectively. P-values were calculated using the Mann-Whitney test. **, $P < 0.01$. Data in A–F are representative of at least two independent experiments. Data in G and H were pooled from two independent experiments.

implying that enhanced PIP_3 production does not necessarily alter synaptic organization. Importantly, suppression of PTEN did not affect IS size in cells lacking Dock2$^{-/-}$ (Fig. 7 C), confirming that PIP_3 functions upstream of Dock2 in this pathway. Collectively, these results indicate that PIP_3-dependent localization of Dock2/Elmo plays a pivotal role in organizing F-actin at the IS.

PI3K–Dock2 signaling modulates CTL killing efficiency

Synaptic architecture is thought to play a central role in CTL killing responses by promoting adhesion to the APC and fusion of lytic granules containing perforin and granzyme with the synaptic membrane (Stinchcombe and Griffiths, 2007). Accordingly, we examined whether perturbations in PI3K-Dock2 signaling affected cytotoxicity. CTLs expressing shRNA against Dock2 exhibited significantly reduced target cell lysis (Fig. 8, A and B). TCR-induced degranulation and granzyme B expression were normal in these cells (Fig. 8, C and D), however, indicating that the observed killing phenotype did not result from defective CTL differentiation or TCR signaling. Rather, these results suggested that contacts formed in the absence of Dock2 lacked the structural integrity required for robust engagement of the APC. Consistent with this interpretation, conjugate formation with target cells was impaired in Dock2-deficient CTLs (Fig. 8 E). We observed a similar adhesion phenotype after wortmannin treatment (Fig. 8 F), further indicating that PI3K-Dock2 signaling is necessary for the formation of robust cytolytic synapses.

Unfortunately, we were unable to investigate killing responses in wortmannin-treated cells because the compound profoundly inhibited degranulation in our hands, consistent with previous results (Robertson et al., 2005). We did, however, analyze CTLs expressing shRNA against PTEN, which we expected to boost PI3K signaling. Cytotoxicity was dramatically enhanced in these cells (Fig. 8, A and B), despite no changes in TCR-induced degranulation and granzyme B expression (Fig. 8, C and D). CTLs lacking PTEN also killed target cells faster than wild-type controls (Fig. 8 B). Surprisingly, loss of PTEN had no effect on conjugate formation (Fig. 8 E), indicating that their enhanced killing activity did not result from an overall increase in synaptic adhesion.

To further explore the effects of Dock2 and PTEN on cytotoxicity, we imaged OT-1 CTLs together with target cells in polydimethylsiloxane (PDMS) microwells designed to block the formation of multicellular clusters. Cell death was monitored using propidium iodide (PI), a fluorescent DNA intercalating reagent that incorporates rapidly into lysed cells (Purbhoo et al., 2004). In this manner, we were able to quantify the frequency of target cell killing induced by "monogamous" interactions involving one T cell and one target cell over a period of ~8 h (Fig. 8, G and H). Whereas 13.5% of conjugates

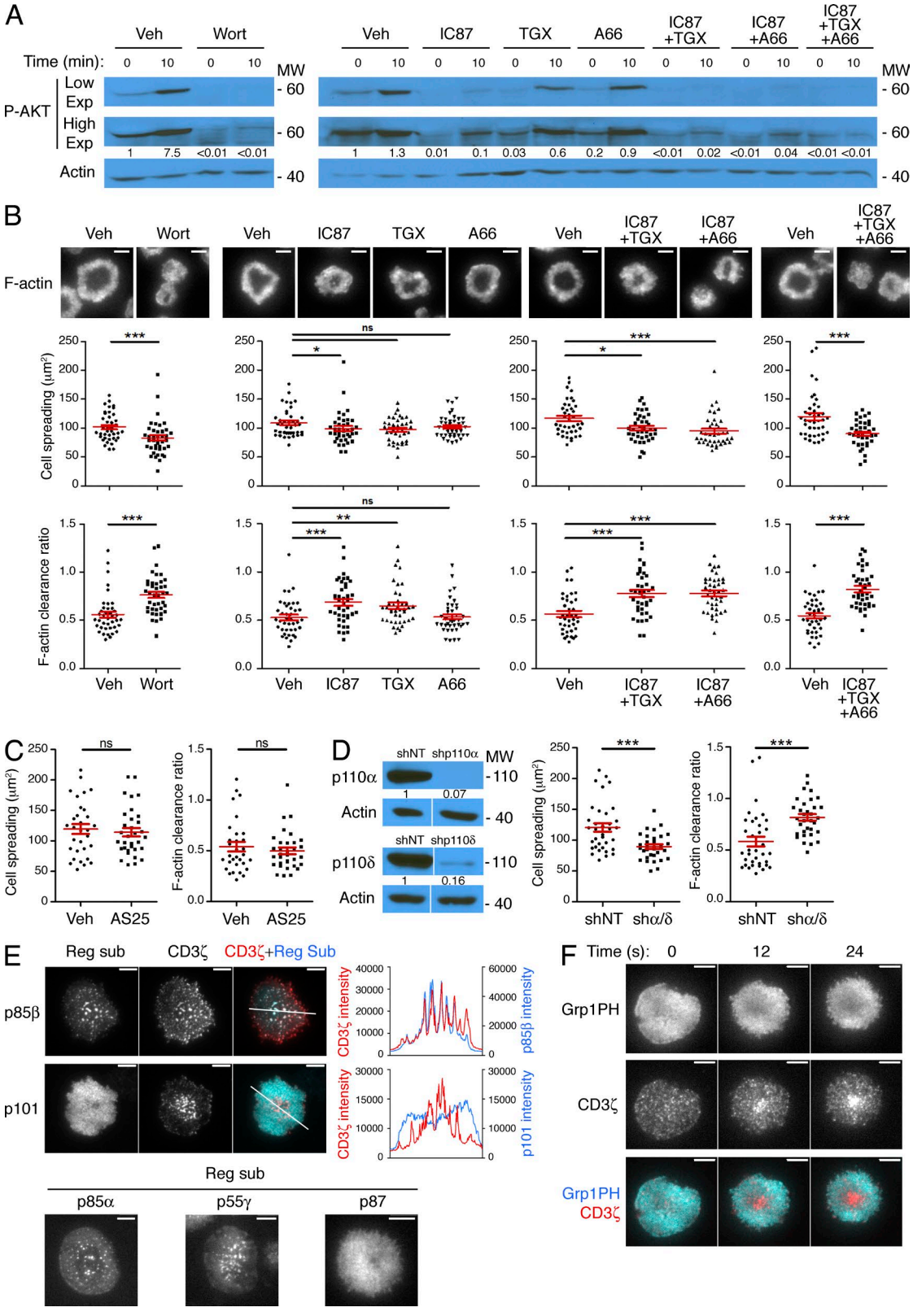

Figure 9. PIP_3-dependent synaptic remodeling is largely mediated by PI3Kδ. (A and B) OT-1 CTLs were pretreated with isoform-specific class IA PI3K inhibitors (alone or in combination) or vehicle controls (Veh) and then stimulated for the indicated times on lipid bilayers containing pMHC and ICAM-1. (A) P-AKT levels were assessed by immunoblot. High and low film exposures are shown. Numbers denote corrected, normalized amounts of P-AKT. (B) Cell spreading and F-actin clearance ratio were assessed after phalloidin-staining (n = 40 cells). Representative TIRF images are shown above,

containing control T cells were associated with a killing event, target cell death was observed in only 2.3% of the conjugates formed by CTLs expressing shRNA against Dock2. PTEN-deficient CTLs, in contrast, lysed target cells in over half (53.9%) of the conjugates they formed. Suppression of PTEN also led to an ∼35% increase in killing rate (Fig. 8 H), quantified by determining the time delay between conjugate formation and target cell death. This acceleration in killing was associated with a reduction in the average duration of CTL–target cell contacts (unpublished data), possibly reflecting an inclination of CTLs to dissociate from dead or dying target cells. Collectively, these results indicate that PIP_3 and Dock2-dependent F-actin dynamics at the IS control the efficiency of target cell killing.

PI3K-dependent F-actin remodeling is largely mediated by PI3Kδ

Class I PI3Ks exist as obligate heterodimers containing one catalytic and one regulatory subunit (Fruman and Bismuth, 2009). Class IA catalytic subunits (p110α, p110β, and p110δ) pair with regulatory subunits in the p85/p55 family, which contain pTyr-binding SH2 domains. In contrast, the lone class IB isoform, p110γ, associates with p101/p87 adaptors and signals downstream of G protein–coupled receptors. To identify which PI3K is primarily responsible for PIP_3 accumulation at the IS, we treated OT-1 CTLs with isoform-specific inhibitors (Fig. 9 A). The p110δ inhibitor IC87114 strongly suppressed TCR-induced phosphorylation of AKT, although not to the same extent as wortmannin. TGX221, a p110β inhibitor which affects p110δ to a lesser extent, reduced phospho-AKT (P-AKT) levels somewhat, whereas A66, which targets p110α, had no observable effect on its own. A252424, a small molecule inhibitor of p110γ, also had no effect on TCR-induced P-AKT (unpublished data), arguing against a role for class IB PI3K. Interestingly, the residual TCR-induced PI3K activity observed in the presence of IC87114 could be further reduced by the addition of A66 or TGX221, suggesting that both p110α and p110β contribute to p110δ-independent PIP_3 production (Fig. 9 A). Indeed, simultaneous treatment with IC87114, TGX221, and A66 completely abrogated AKT phosphorylation.

We observed a similar pattern of results when we examined the synaptic architecture of inhibitor-treated cells (Fig. 9, B and C). Neither A66 nor AS252424 affected IS size and F-actin clearance ratio. In contrast, IC87114 induced significant, albeit small, changes in both parameters. TGX221 also disrupted synaptic F-actin somewhat, most likely due to partial inhibition of p110δ. Treatment with combinations of IC87114 and either TGX221 or A66 induced substantially larger defects in cell spreading and synaptic organization, and application of all three compounds together produced a phenotype as severe as that of wortmannin. These results imply that PI3Kδ drives synaptic PIP_3 accumulation together with either PI3Kα or PI3Kβ. Consistent with this interpretation, shRNA-mediated suppression of p110δ together with p110α strongly inhibited both cell spreading and F-actin ring formation (Fig. 9 D).

We also analyzed the localization of class IA and class IB PI3Ks using CTLs transduced with GFP-labeled p85α, p85β, or p55γ (to label class IA isoforms) or GFP-labeled p87 or p101 (for class IB). TIRF analysis revealed that p101 and p87 adopted broad and rather nonspecific distributions (Fig. 9 E). In contrast, p85α, p85β, and p55γ formed distinct microclusters in the plasma membrane that trafficked toward the center of the IS (Fig. 9 E; and Videos 5 and 6). Because activated TCR complexes also form centripetally motile microclusters (Dustin et al., 2010), we investigated whether p85/p55 colocalized with the TCR. Indeed, labeled p85α, p85β, and p55γ overlapped extensively with CD3ζ-RFP, a marker of the TCR (Fig. 9 E and not depicted). These results strongly suggest that class IA PI3K isoforms are recruited directly to TCR microclusters, consistent with a role in TCR-induced PIP_3 production.

It is generally thought that signaling from TCR microclusters, although strong in the periphery of the IS, is extinguished as they coalesce at the center (Campi et al., 2005; Yokosuka et al., 2005; Varma et al., 2006; Vardhana et al., 2010). Consistent with this model, we observed that accumulation of PIP_3 into an annular pattern coincided with formation of a large central cluster of TCR (Fig. 9 F and Video 7). Collectively with the loss-of-function experiments described above, these results indicate that synaptic PIP_3 is generated by class IA PI3Ks associated with TCR microclusters in the periphery of the IS.

Ras controls synaptic PI3K activation

Because TCR signaling is known to induce robust Ras activation (Mor and Philips, 2006), we investigated whether Ras might regulate PI3K-dependent F-actin remodeling at the IS. CTLs expressing a constitutively active Ras mutant (V12Ras) displayed a substantial increase in cell spreading on stimulatory

with quantification below. (C) OT-1 CTLs were pretreated with AS252424 (AS25) or vehicle control (Veh) and then stimulated and imaged as described in B. Quantification of cell spreading and F-actin clearance ratio are shown ($n > 30$ cells). (D) OT-1 CTLs expressing shRNA against p110α together with p110δ or nontargeting control shRNA (shNT) were stimulated and imaged as described in B. Left, transduced cells were probed for p110α and p110δ by immunoblot. Numbers denote corrected, normalized amounts of p110α and p110δ. Right, quantification of cell spreading and F-actin clearance ratio ($n \geq 33$ cells). (E) Top, OT-1 CTLs expressing RFP-tagged CD3ζ together with the indicated GFP-labeled PI3K regulatory subunits were fixed on stimulatory bilayers. Top left, representative TIRF images are shown. Top right, linescans (derived from the white lines shown on the TIRF images) showing colocalization between CD3ζ and the PI3K regulatory subunits. Bottom, representative TIRF images of OT-1 CTLs expressing the indicated GFP-labeled PI3K regulatory subunits after fixation on stimulatory bilayers. (F) OT-1 CTLs expressing RFP-labeled CD3ζ together with GFP-labeled Grp1PH were imaged by TIRF microscopy on bilayers containing pMHC and ICAM-1. A representative time-lapse montage is shown (12-s intervals). Bars, 5 µm. In scatter plots, red lines and error bars denote the mean and SEM, respectively. P-values were calculated using the Mann-Whitney test. ***, $P < 0.001$, **, $P < 0.01$, *, $P \leq 0.05$, and ns, $P > 0.05$. Data in A–D are representative of at least two independent experiments. Images in E and F are representative of at least 17 cells imaged over at least two independent experiments.

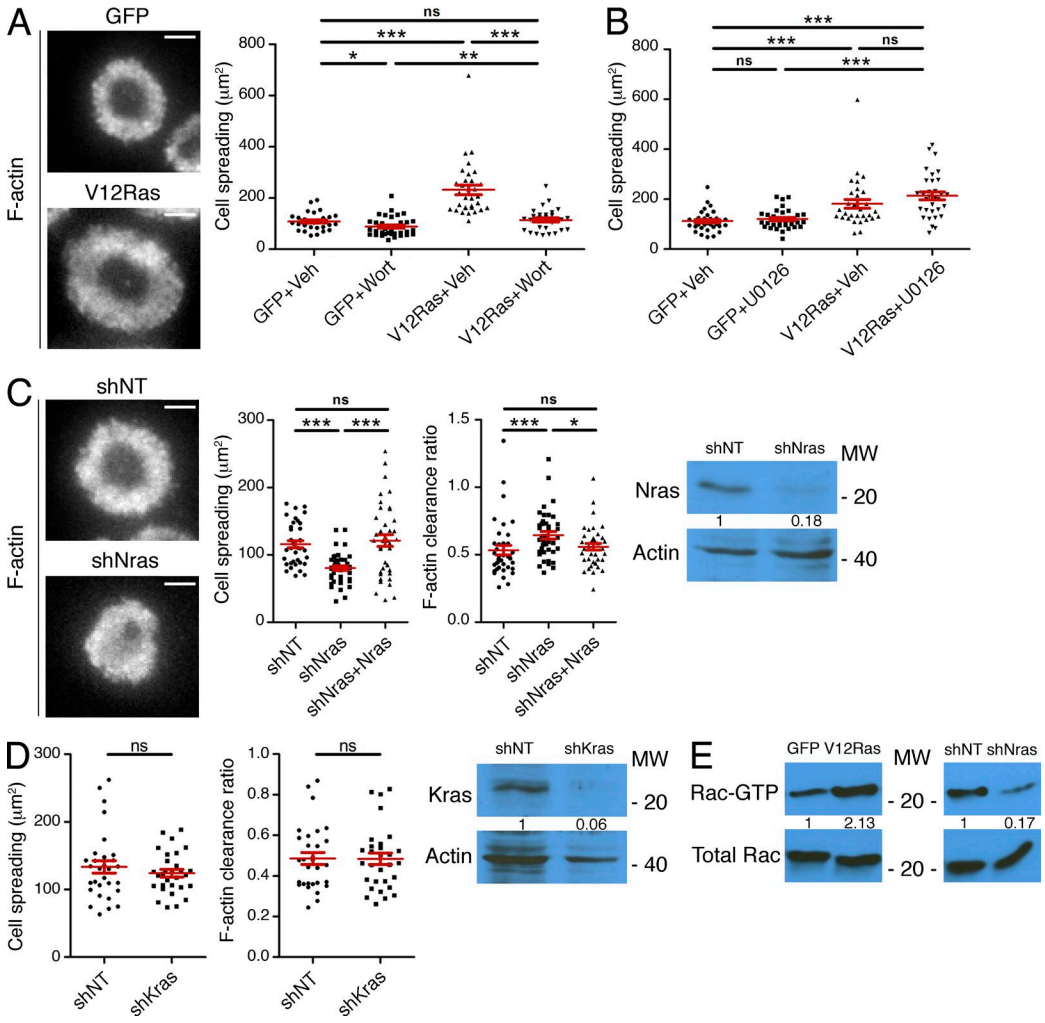

Figure 10. Ras drives PI3K activation and F-actin remodeling at the IS. (A and B) OT-1 CTLs expressing GFP-labeled V12Ras or GFP alone were stimulated on lipid bilayers containing pMHC and ICAM-1 in the presence of either wortmannin (Wort; A) or U0126 (B) as indicated (Veh = vehicle control). Cells were then fixed and phalloidin-stained. Quantification of cell spreading is shown ($n \geq 30$ cells). Representative TIRF images of V12Ras-expressing cells and GFP-expressing controls are shown to the left in A. (C) OT-1 CTLs were transduced with nontargeting control shRNA (shNT) or shRNA specific for Nras either in the presence or the absence of shRNA-resistant, GFP-labeled Nras. Cells were then stimulated on bilayers containing pMHC and ICAM-1, fixed, and stained with phalloidin. Left, representative TIRF images are shown. Middle, quantification of cell spreading and F-actin clearance ratio ($n \geq 37$ cells). Right, Nras protein expression by immunoblot. Numbers denote corrected, normalized amounts of Nras. (D) OT-1 CTLs expressing nontargeting control shRNA (shNT) or shRNA specific for Kras were stimulated on bilayers containing pMHC and ICAM-1, fixed, and stained with phalloidin. Left, quantification of cell spreading and F-actin clearance ratio ($n = 30$ cells). Right, Kras protein expression by immunoblot. Numbers denote corrected, normalized amounts of Kras. (E) OT-1 CTLs expressing V12ras (left) or shNras (right) were stimulated, along with the indicated controls, using beads coated with pMHC and ICAM-1. Cell extracts were incubated with GST-PAK1-PBD, and Rac activation was analyzed by immunoblot. Numbers denote corrected, normalized amounts of activated Rac. Bars, 5 µm. In scatter plots, red lines and error bars denote the mean and SEM, respectively. P-values were calculated using the Mann-Whitney test (two-tailed). ***, $P < 0.001$, **, $P < 0.01$, *, $P \leq 0.05$, and ns, $P > 0.05$. Data are representative of at least two independent experiments.

bilayers (Fig. 10 A), similar to the phenotype observed in PTEN-deficient cells. This increase in IS size could be reversed by wortmannin, indicating that PI3K operated downstream of V12Ras in these experiments. Although Ras also activates MAP kinase signaling (Mor and Philips, 2006), the MAP kinase pathway inhibitor U0126 did not affect the cell spreading phenotype induced by V12Ras (Fig. 10 B). Hence, we conclude that V12Ras functions through PI3K, rather than the MAP kinase cascade, to influence synaptic architecture.

We also analyzed OT-1 CTLs expressing shRNA against Nras, the predominant Ras isoform in T cells (Leon et al., 1987; Perez de Castro et al., 2004). Nras depletion induced defects in both F-actin ring formation and cell spreading (Fig. 10 C). This phenotype was specific, as it was reversed by transduction of an shRNA-resistant version of Nras (Fig. 10 C). Notably, suppression of Kras had no effect on IS growth and organization, presumably because it is expressed at substantially lower levels than Nras in T cells (Fig. 10 D).

These results implied that Nras plays a major role in controlling PIP_3-dependent activation of Rac. Consistent with this interpretation, TCR-induced Rac activation was markedly enhanced in CTLs expressing V12Ras and markedly reduced in CTLs lacking Nras (Fig. 10 E). Collectively, our data demonstrate that Ras, predominantly the Nras isoform, controls PI3K and Rac activity downstream of the TCR.

DISCUSSION

Although it has been known for some time that TCR signaling induces robust F-actin remodeling at the IS, the mechanisms controlling this process have remained mysterious. Here, we demonstrate that annular PIP_3 accumulation, generated downstream of Ras and class IA PI3K, is crucial for shaping synaptic F-actin and the effector responses that depend on it. Previous studies have highlighted the value of Ras and PI3K for TCR-induced transcriptional responses, proliferation, and survival (Mor and Philips, 2006; Fruman and Bismuth, 2009). Our results reveal that both proteins also function as important cytoskeletal organizers.

The Dock2/Elmo complex plays a central role in leukocyte migration by promoting protrusive actin polymerization at the leading edge (Fukui et al., 2001; Nombela-Arrieta et al., 2004; Nishikimi et al., 2009). Our work demonstrates that Dock2/Elmo also drives F-actin growth in the IS. The parallels between the radially symmetric lamellipodium observed at the IS and the oriented lamellipodium seen in motile leukocytes have been noted (Dustin, 2007). The implication of Dock2 as a crucial component of both structures confirms and extends this concept. That being said, there are significant differences in the way Dock2/Elmo is localized in motile leukocytes relative to synaptically engaged T cells. In migrating neutrophils, for instance, Dock2 accumulation at the leading edge is primarily driven by phosphatidic acid, with PIP_3 playing only a minor role (Nishikimi et al., 2009). Dock2 is also capable of controlling T cell and B cell migration in a largely PI3K-independent manner (Nombela-Arrieta et al., 2004). In contrast, our results demonstrate that PIP_3 accounts for the majority of TCR-induced Dock2 recruitment and Rac activation at the IS. It is interesting that the mechanisms regulating Dock2/Elmo during T cell activation should differ from those used during chemotaxis. These alternative strategies could help T cells delineate distinct morphological states that otherwise use many of the same protein regulators.

Although Dock2 is clearly pivotal for activating Rac and specifying F-actin growth at the IS, the persistence of F-actin ring formation in the absence of Dock2 implies the existence of additional PIP_3-regulated factors that signal through Rac to promote synaptic organization. A particularly intriguing candidate is Tiam1, a Rac-specific GEF that binds to PIP_3 via its N-terminal PH domain (Rameh et al., 1997). Recent work has established that Tiam1 can activate Rac downstream of LFA-1 in T cells (Grönholm et al., 2011), although it remains unclear whether PIP_3 is involved. Tiam1 also associates with the Par (partitioning defective) polarity complex (Chen and Macara, 2005; Nishimura et al., 2005), which accumulates at the IS and contributes to the establishment of cell polarity (Ludford-Menting et al., 2005). Whether the Par complex and Tiam1 influence the organization of synaptic F-actin has not been explored and remains an interesting topic for future investigation.

The colocalization we observed between p85/p55 and the TCR in microclusters is quite intriguing in light of prior work indicating that class IA PI3Ks can be stimulated allosterically by pTyr-containing peptides (Carpenter et al., 1993; Holt et al., 1994). The TCR signaling complex contains several phosphoproteins that could potentially engage PI3K, including LAT and Slp76, two scaffolding molecules known to interact with p85 in a pTyr-dependent manner (Zhang et al., 1998; Shim et al., 2004, 2011). Hence, we favor a model in which early TCR signaling drives pTyr-mediated recruitment and allosteric activation of class IA PI3K in centripetally motile microclusters. Once localized to the plasma membrane in this manner, PI3K encounters Ras-GTP, becomes fully activated, and generates PIP_3. Importantly, we expect microcluster-associated PI3K to be active only in the periphery of the IS because signaling from TCR microclusters is extinguished as they coalesce in the center (Campi et al., 2005; Yokosuka et al., 2005; Varma et al., 2006; Vardhana et al., 2010). Hence, this model is consistent with the annular pattern of PIP_3 we have observed.

Ras is C-terminally prenylated and palmitoylated, and Ras activation is often localized to specific cellular membranes (Mor and Philips, 2006). In T cells, the degree of this compartmentalization depends on the nature of the stimulus. Thus, whereas engagement of the TCR either alone or in combination with CD28 activates Ras exclusively in the Golgi apparatus, simultaneous stimulation of the TCR and LFA-1 drives Ras activation at the plasma membrane (Mor et al., 2007). It is striking that these stimulus criteria, namely co-engagement of the TCR and LFA-1, are identical to the requirements for stable F-actin ring formation in our system. Class IA PI3K predominantly functions at the plasma membrane, which is enriched in phosphatidylinositol bisphosphate relative to other compartments (Czech, 2000). Hence, it is not surprising that stimulatory regimes inducing Ras activation at the plasma membrane should be the most effective at promoting PI3K-dependent F-actin remodeling.

It is remarkable that suppression of Dock2 or PTEN affected cytotoxicity so strongly without significantly altering TCR-induced degranulation. These results suggest that PI3K-Dock2 signaling modulates the cytolytic potential of degranulation rather than its overall level. Given the presumed importance of synaptic F-actin for directional secretion, it is tempting to speculate that perturbations in the PI3K-Dock2 pathway might modify synaptic targeting of lytic granules. We have found, however, that granule polarization toward the synapse is unaffected by loss of Dock2 or PTEN (unpublished data). Nevertheless, it remains possible that the actual release of these granules does change under these conditions. Alternatively, by modulating the strength of the IS, perturbations in PI3K-Dock2 signaling may affect the ability of CTLs to exert force on the APC membrane and thereby alter cytotoxicity. Both possibilities represent interesting avenues for future research.

Our functional results with PTEN-deficient CTLs indicate that cellular cytotoxicity can be boosted to supraphysiological levels. This is consistent with previous studies suggesting that wild-type CTLs are relatively inefficient killers that possess untapped cytolytic capacity (Loeser et al., 2007; Budhu et al., 2010; Riese et al., 2013). Under normal circumstances, restraining CTL function may be important for the general health of an organism. Indeed, mice lacking PTEN specifically in peripheral T cells develop multi-organ autoimmune disease (Liu et al., 2010). However, there are therapeutic contexts, such as the adoptive transfer of tumor-specific T cells (Sadelain et al., 2003), in which the ability to enhance CTL function might be very advantageous. Indeed, CTLs lacking negative regulators of the TCR signaling network show markedly improved anti-tumor responses in certain mouse models (Loeser et al., 2007; Stromnes et al., 2010; Riese et al., 2013). In that regard, it will be interesting to investigate whether PTEN-deficient CTLs mount more effective immune responses in vivo. Interestingly, CTLs lacking SHIP-1, a lipid phosphatase which targets PIP_3 at the 5′ position, also display enhanced killing responses (Tarasenko et al., 2007), although to a lesser extent than cells lacking PTEN. Hence, up-regulation of PI3K signaling could serve as a general mechanism to boost lymphocyte cytotoxicity.

We showed previously that MTOC polarization toward the APC is driven by the accumulation of diacylglycerol at the IS (Quann et al., 2009). Here, we demonstrate that a distinct lipid second messenger, PIP_3, plays a crucial role in shaping synaptic F-actin. It is remarkable that T cells should use lipid second messenger signaling to dictate the polarity and architecture of both the microtubule and actin cytoskeletons during IS formation. Studies in migrating cells have demonstrated that plasma membrane lipid gradients can be generated quickly and are highly responsive to change (Funamoto et al., 2002; Iijima and Devreotes, 2002; Wang et al., 2002). This makes them well suited for the patterning of dynamic cytoskeletal structures. It seems likely that systems analogous to the ones we have characterized in T cells are used by other cell types to shape F-actin and microtubule architecture during the formation of specialized cell–cell contacts.

MATERIALS AND METHODS

Constructs and inhibitors. Coding sequences for GFP-labeled Grp1PH, GFP-labeled Dyn1PH, and RFP-Ruby–labeled Lifeact were amplified by PCR from pEGFP-C1-Grp1PH, pEGFP-C1-Dyn1PH, and pmRFPruby-N1-Lifeact, respectively, and then cloned into a modified retroviral expression vector (pMSCV). Coding sequences for mouse WAVE2 and CD3ζ were cloned into pMSCV upstream of GFP and RFP, respectively. Coding sequences of mouse p85α, p85β, p55γ, p87, p101, Dock2, Dock2-ΔDHR1, and Elmo1 were cloned into a shuttle vector derived from pTOPO (Invitrogen) downstream of GFP (NT-GFP-TOPO). Fragments encoding the fluorescent fusion proteins were then subcloned in pMSCV. Constitutively active Rac1 and Nras (V12Rac1, V12Nras, G12V mutation) were created by PCR-based mutagenesis, cloned into NT-GFP-TOPO, and then subcloned as GFP fusions into pMSCV. V12Hras was amplified by PCR from pBABE-V12Hras, and subcloned as a GFP-V12Hras fragment into pMSCV. V12Nras and V12Hras had equivalent effects on synaptic architecture and were used interchangeably. shRNAs specific for Rac1, Rac2, Dock2, PTEN, p110α, p110δ, Nras, and Kras were cloned into LMP vectors (Open Biosystems) containing fluorescent protein markers (either GFP or CFP) appropriate for each experiment. To inhibit PI3K or MAPK signaling, OT-1 CTLs were pretreated with 500 nM wortmannin (Sigma-Aldrich), 1 μM IC87114/TGX221/A66/AS252424 (Symansis), or 10 μM U0126 (EMD) for 30 min at 37°C.

Cells and retroviral transduction. The animal protocols used for this study were approved by the Institutional Animal Care and Use Committee of Memorial Sloan-Kettering Cancer Center. Primary helper T cell and CTL blasts were prepared from Dock2$^{-/-}$ 2B4αβ (Sanui et al., 2003) and OT-1αβ transgenic mice (Taconic), respectively. Lymphocytes from these mice were mixed with irradiated congenic splenocytes pulsed with 5 μM moth cytochrome $c_{88\text{-}103}$ peptide (MCC, helper T cells) or 100 nM ovalbumin$_{257\text{-}264}$ (OVA, CTLs) and cultured in RPMI medium containing 10% (vol/vol) FCS. Cells were supplemented with 30 IU/ml IL-2 after 24 h and were split as needed in RPMI containing IL-2. RMA-s mouse tumor cells were maintained in RPMI containing 10% (vol/vol) FCS. For retroviral transduction, Phoenix E cells were transfected with pMSCV expression vectors and packaging plasmids by the calcium phosphate method. Ecotropic viral supernatants were collected after 48 h at 37°C and added to T cell blasts 2 or 3 d after primary peptide stimulation. Mixtures were centrifuged at 1,400 *g* in the presence of 4 μg/ml polybrene at 35°C. T cells were then split 1:3 in medium containing IL-2.

Pulldown assays and immunoblot analysis. For pulldown assays, serum-starved T cells were incubated with streptavidin-coated polystyrene beads (Spherotech) loaded with 1 μg/ml each of the biotinylated proteins ICAM-1 and H-2K^b-OVA$_{257\text{-}264}$ in 150 μl RPMI for the indicated times at 37°C (ratio = 1:1), and immediately lysed by adding 150 μl of cold 2× lysis buffer (100 mM Hepes, pH 7.4, 300 mM NaCl, 2% Triton X-100, 20 mM $MgCl_2$, and protease inhibitors). To assess Rac activation, cell extracts were incubated with the PAK1-PBD fused to glutathione S-transferase (GST) at 4°C for 1 h. GST-PAK1-PBD–bound proteins were analyzed by SDS-PAGE, and blots were probed with anti-Rac antibodies (clone 23A8; Abcam). To assess shRNA knockdown efficiency, equal numbers of OT-1 CTLs infected with either nontargeting shRNA or shRNA specific for the protein of interest were lysed by adding cold cell lysis buffer containing 10 mM TrisHCl, 5 mM EDTA, 1% NP-40, 0.5% sodium deoxycholate, and 0.15 M NaCl. Samples were analyzed by immunoblot using the following antibodies: anti-Rac1 mAb (clone ARC03, Cytoskeleton), anti-Rac2 mAb (clone C-11; Santa Cruz Biotechnology, Inc.), anti-Dock2 polyclonal Ab (Millipore), anti-PTEN mAb (clone D4.3; Cell Signaling Technology), anti-p110α mAb (clone C73F8; Cell Signaling Technology), anti-p110δ mAb (clone EPR386; Abcam), anti-Kras mAb (clone F234; Santa Cruz Biotechnology, Inc.), and anti-Nras mAb (clone F155; Santa Cruz Biotechnology, Inc.). Inhibition of PI3K and MAP kinase signaling in OT-1 CTLs was assessed by immunoblot for P-AKT (anti-P-AKT [Ser473] Ab; Cell Signaling Technology) and P-Erk1/2 (P-Thr202/Tyr204; clone 20G11; Cell Signaling Technology), respectively, after stimulation on lipid bilayers containing pMHC and ICAM-1 (see TIRF imaging experiments). Cells were lysed as described for shRNA-infected cells. Immunoblots were quantified in ImageJ by calculating the ratio between the band of interest and a standard band (total Rac, actin, or tubulin) in each lane. For quantification of activated Rac, P-Erk1/2, and P-AKT, values were normalized using samples from unstimulated cells or cells expressing control constructs (e.g., GFP alone or nontargeting shRNA) as indicated. For validation of shRNA knockdown, values were normalized using samples from cells expressing nontargeting shRNA.

Killing assays, degranulation, and conjugate formation. RMA-s target cells labeled with the membrane dye PKH26 (Sigma-Aldrich) were pulsed with 100 nM OVA and mixed in 96-well plates with OT-1 CTLs transduced with nontargeting shRNA or shRNA specific for Dock2 or PTEN. For killing assays, E:T ratios were 0.5:1, 1:1, 2:1, and 4:1, and cells were incubated at 37°C for 0–6 h. 2.5 mM EDTA was then added to disrupt conjugate formation and specific lysis of PKH26$^+$ target cells was assessed by flow

cytometry as previously described (Purbhoo et al., 2004). For degranulation assays, the E/T ratio was 1:1 and cells were incubated at 37°C for 0–60 min in the presence of Alexa Fluor 647–labeled mAb to CD107a (1 µg/ml; clone eBio1D4B; eBioscience). Conjugates were then disrupted by the addition of 2.5 mM EDTA, and CD107a staining assessed by flow cytometry after gating out $PKH26^+$ target cells. Conjugate formation was analyzed after mixing GFP^+ OT-1 CTLs with $PKH26^+$ target cells for 0–60 min at 37°C. Conjugates were visualized as GFP^+PKH26^+ entities by flow cytometry. % conjugates = $[GFP^+PKH26^+/(GFP^+PKH26^- + GFP^+PKH26^+)]$. For intracellular granzyme B staining, T cells were fixed with 2% PFA, permeabilized with 0.1% saponin (diluted in PBS 1× containing 1% BSA), and stained with anti–granzyme B coupled to APC (clone GB11; Invitrogen).

Image analysis of single cell killing. PDMS grids containing 50 × 50 × 25–µm wells were submerged in imaging medium and seeded with RMA-s cells that had been pulsed with 100 nM OVA. In general, individual wells contained 1–3 RMA-s cells. 1 µg/ml PI was added to the medium to enable real-time labeling of dead cells. Then, CTLs expressing control shRNA or shRNA against Dock2 or PTEN together with GFP were added and the cells imaged using a 10× objective lens (Carl Zeiss) at 2-min intervals for 8 h. Brightfield, GFP, and PI images were collected at each time point. Quantification was restricted to target cells forming synapses with only one T cell during the first 6 h of the imaging experiment. All cells in this category were scored for the time of initial IS formation and also for the initial appearance of PI signal above background.

TIRF imaging. Supported lipid bilayers containing streptavidin were coated with biotinylated proteins as previously described (Abeyweera et al., 2011). For 2B4 T cells, 1 µg/ml each of biotinylated MCC-I-E^k and ICAM-1 were used; for OT-1 cells, 1 µg/ml of biotinylated OVA-H-$2K^b$ in combination with 1 µg/ml ICAM-1, B7.1, or a nonstimulatory null pMHC was used. In live experiments, TIRF images of fluorescently labeled T cells in contact with bilayers were collected every 3 s for 6 min with a 60× objective lens (1.45 NA; Olympus) using 488 and 561 nm lasers (Melles Griot) for imaging of GFP and RFP, respectively. For fixed samples, T cells were incubated on stimulatory bilayers for 10 min at 37°C, fixed by adding 4% paraformaldehyde for 5 min, and imaged after neutralization with 15 mM NH_4Cl. For phalloidin staining, fixed cells were permeabilized with 0.1% Triton X-100 for 5 min, followed by incubation in PBS solution supplemented with 5% BSA for 20 min at 37°C. Cells were then incubated for 30 min with 0.1 U/ml Alexa Fluor 594–labeled phalloidin dissolved in PBS supplemented with 5% BSA. Live imaging of p85α and p85β at the IS was performed using a 150× objective lens (1.45 NA; Olympus). shRNA-transduced cells were identified by GFP and/or CFP expression. For Ca^{2+} flux assays, T cells were loaded with 5 µg/ml Fura-2AM (Invitrogen), followed by imaging on stimulatory bilayers using a 40× objective lens (1.35 NA; Olympus). Differential interference contrast and Fura-2 images were collected every 30 s for 30 min. TCR-induced polarization of the MTOC was assessed by TCR photoactivation as previously described (Quann et al., 2009) using glass surfaces coated with 0.25 µg/ml of photocaged MCC-I-E^k, 2.75 µg/ml of nonstimulatory null pMHC, and 0.5 µg/ml of antibodies against H-$2K^k$ (36–7-5; BD).

Conjugate imaging. RMA-s target cells pulsed with 100 nM OVA were mixed in complete RPMI at a 1:2 ratio with either OT-1 CTLs expressing shRNA (nontargeting shRNA or shRNA specific for Dock2 or PTEN) or CFSE-labeled OT-1 cells pretreated with wortmannin (Wort) or vehicle control. Cells were pelleted and incubated for 10 min at 37°C. Conjugates were then resuspended in warm PBS, transferred into poly-L-lysine–coated Millicell EZ slides (EMD Millipore), and incubated for 5 min at 37°C. Cells were then fixed, permeabilized, and stained with Alexa Fluor 594–labeled phalloidin (see TIRF imaging experiments). Slides were then mounted with Mowiol (EMD Millipore) and analyzed using a fluorescence confocal microscope (Upright; Leica). Z-projections and 3D reconstructions were assembled using Imaris Imaging software.

Image analysis. Imaging data were analyzed using SlideBook software, Excel (Microsoft), Prism (GraphPad Software), and Imaris. Cell spreading on bilayers was determined by calculating the cell area (in square micrometers) after intensity thresholding of the Alexa Fluor 594–labeled phalloidin signal. Quantification of clearance ratio was performed using two perpendicular linescans for each cell. For each linescan, the background-corrected mean fluorescence intensity (MFI) at the edges (positions F1 and F2) of the IS was compared with the background-corrected MFI of three equally spaced central positions (F3, F4, and F5) as follows: mean(F3 + F4 + F5)/mean(F1 + F2). Clearance ratios derived from the two perpendicular linescans were averaged to yield a clearance ratio for the cell in question. Analysis of single cell Ca^{2+} flux was performed by normalizing the Fura ratio of each cell using the last image before the initial rise in Ca^{2+}. MTOC reorientation in response to photoactivation was quantified by calculating the distance between the MTOC and the center of the irradiated region as a function of time. Synapse size in CTL–target cell conjugates was quantified by averaging the values of two perpendicular measurements of IS diameter made using 3D reconstructions. Accumulation of F-actin and Dock2 at the CTL-target cell IS (MFI ratio) was quantified by determining the ratio of the MFI at the IS to the MFI at the back of the T cell, calculated using Z-projections. Data for conjugate analysis was pooled from two independent experiments. All other datasets used for quantification comprised images recorded on the same day.

Online supplemental material. Videos 1, 2, 3, and 4 show the localization of F-actin (labeled with Lifeact-RFP) during IS formation together with WAVE2 (WAVE2-GFP), Dock2/Elmo (GFP-Elmo1), PIP_3 (GFP-Grp1PH), and GFP-DynPH (PH domain that does not bind to PIP_3), respectively. Videos 5 and 6 show the localization of GFP-p85α and GFP-p85β, respectively, in microclusters during IS formation. Video 7 shows the localization of GFP-Grp1PH together with CD3ζ-RFP (to label the TCR). Online supplemental material is available at http://www.jem.org/cgi/content/full/jem.20131324/DC1.

We thank X. Liu for assistance with shRNA transduction; M. Lemmon (University of Pennsylvania), A. Nishikimi (Kyushu University), R. Wedlich-Söldner (IMPRS), and A. Hall (MSKCC) for constructs; the Molecular Cytology Core Facility at MSKCC for confocal microscopy; A. Hall and A. Rudensky (MSKCC) for critical reading of the manuscript; and members of the Huse and M.O. Li laboratories for advice.

This study was supported in part by the U.S. National Institutes of Health (R01-AI087644), the Searle Scholars Program, and the Cancer Research Institute (M. Huse).

The authors have no conflicting interests.

Submitted: 25 June 2013
Accepted: 7 October 2013

REFERENCES

Abeyweera, T.P., E. Merino, and M. Huse. 2011. Inhibitory signaling blocks activating receptor clustering and induces cytoskeletal retraction in natural killer cells. *J. Cell Biol.* 192:675–690. http://dx.doi.org/10.1083/jcb.201009135

Acuto, O., and F. Michel. 2003. CD28-mediated co-stimulation: a quantitative support for TCR signalling. *Nat. Rev. Immunol.* 3:939–951. http://dx.doi.org/10.1038/nri1248

Alcázar, I., M. Marqués, A. Kumar, E. Hirsch, M. Wymann, A.C. Carrera, and D.F. Barber. 2007. Phosphoinositide 3-kinase γ participates in T cell receptor-induced T cell activation. *J. Exp. Med.* 204:2977–2987. http://dx.doi.org/10.1084/jem.20070366

Anikeeva, N., K. Somersalo, T.N. Sims, V.K. Thomas, M.L. Dustin, and Y. Sykulev. 2005. Distinct role of lymphocyte function-associated antigen-1 in mediating effective cytolytic activity by cytotoxic T lymphocytes. *Proc. Natl. Acad. Sci. USA.* 102:6437–6442. http://dx.doi.org/10.1073/pnas.0502467102

Babich, A., S. Li, R.S. O'Connor, M.C. Milone, B.D. Freedman, and J.K. Burkhardt. 2012. F-actin polymerization and retrograde flow drive sustained PLCγ1 signaling during T cell activation. *J. Cell Biol.* 197:775–787. http://dx.doi.org/10.1083/jcb.201201018

Beemiller, P., J. Jacobelli, and M.F. Krummel. 2012. Integration of the movement of signaling microclusters with cellular motility in immunological synapses. *Nat. Immunol.* 13:787–795. http://dx.doi.org/10.1038/ni.2364

Buckler, J.L., X. Liu, and L.A. Turka. 2008. Regulation of T-cell responses by PTEN. *Immunol. Rev.* 224:239–248. http://dx.doi.org/10.1111/j.1600-065X.2008.00650.x

Budhu, S., J.D. Loike, A. Pandolfi, S. Han, G. Catalano, A. Constantinescu, R. Clynes, and S.C. Silverstein. 2010. $CD8^+$ T cell concentration determines their efficiency in killing cognate antigen-expressing syngeneic mammalian cells in vitro and in mouse tissues. *J. Exp. Med.* 207:223–235. http://dx.doi.org/10.1084/jem.20091279

Bunnell, S.C., V. Kapoor, R.P. Trible, W. Zhang, and L.E. Samelson. 2001. Dynamic actin polymerization drives T cell receptor-induced spreading: a role for the signal transduction adaptor LAT. *Immunity.* 14:315–329. http://dx.doi.org/10.1016/S1074-7613(01)00112-1

Campi, G., R. Varma, and M.L. Dustin. 2005. Actin and agonist MHC-peptide complex-dependent T cell receptor microclusters as scaffolds for signaling. *J. Exp. Med.* 202:1031–1036. http://dx.doi.org/10.1084/jem.20051182

Carpenter, C.L., K.R. Auger, M. Chanudhuri, M. Yoakim, B. Schaffhausen, S. Shoelson, and L.C. Cantley. 1993. Phosphoinositide 3-kinase is activated by phosphopeptides that bind to the SH2 domains of the 85-kDa subunit. *J. Biol. Chem.* 268:9478–9483.

Chen, X., and I.G. Macara. 2005. Par-3 controls tight junction assembly through the Rac exchange factor Tiam1. *Nat. Cell Biol.* 7:262–269. http://dx.doi.org/10.1038/ncb1226

Costello, P.S., M. Gallagher, and D.A. Cantrell. 2002. Sustained and dynamic inositol lipid metabolism inside and outside the immunological synapse. *Nat. Immunol.* 3:1082–1089. http://dx.doi.org/10.1038/ni848

Côté, J.F., and K. Vuori. 2007. GEF what? Dock180 and related proteins help Rac to polarize cells in new ways. *Trends Cell Biol.* 17:383–393. http://dx.doi.org/10.1016/j.tcb.2007.05.001

Czech, M.P. 2000. PIP2 and PIP3: complex roles at the cell surface. *Cell.* 100:603–606. http://dx.doi.org/10.1016/S0092-8674(00)80696-0

Dustin, M.L. 2007. Cell adhesion molecules and actin cytoskeleton at immune synapses and kinapses. *Curr. Opin. Cell Biol.* 19:529–533. http://dx.doi.org/10.1016/j.ceb.2007.08.003

Dustin, M.L., and E.O. Long. 2010. Cytotoxic immunological synapses. *Immunol. Rev.* 235:24–34. http://dx.doi.org/10.1111/j.0105-2896.2010.00904.x

Dustin, M.L., A.K. Chakraborty, and A.S. Shaw. 2010. Understanding the structure and function of the immunological synapse. *Cold Spring Harb. Perspect. Biol.* 2:a002311. http://dx.doi.org/10.1101/cshperspect.a002311

Fruman, D.A., and G. Bismuth. 2009. Fine tuning the immune response with PI3K. *Immunol. Rev.* 228:253–272. http://dx.doi.org/10.1111/j.1600-065X.2008.00750.x

Fukui, Y., O. Hashimoto, T. Sanui, T. Oono, H. Koga, M. Abe, A. Inayoshi, M. Noda, M. Oike, T. Shirai, and T. Sasazuki. 2001. Haematopoietic cell-specific CDM family protein DOCK2 is essential for lymphocyte migration. *Nature.* 412:826–831. http://dx.doi.org/10.1038/35090591

Funamoto, S., R. Meili, S. Lee, L. Parry, and R.A. Firtel. 2002. Spatial and temporal regulation of 3-phosphoinositides by PI 3-kinase and PTEN mediates chemotaxis. *Cell.* 109:611–623. http://dx.doi.org/10.1016/S0092-8674(02)00755-9

Garçon, F., D.T. Patton, J.L. Emery, E. Hirsch, R. Rottapel, T. Sasaki, and K. Okkenhaug. 2008. CD28 provides T-cell costimulation and enhances PI3K activity at the immune synapse independently of its capacity to interact with the p85/p110 heterodimer. *Blood.* 111:1464–1471. http://dx.doi.org/10.1182/blood-2007-08-108050

Genot, E., and D.A. Cantrell. 2000. Ras regulation and function in lymphocytes. *Curr. Opin. Immunol.* 12:289–294. http://dx.doi.org/10.1016/S0952-7915(00)00089-3

Gomez, T.S., and D.D. Billadeau. 2008. T cell activation and the cytoskeleton: you can't have one without the other. *Adv. Immunol.* 97:1–64. http://dx.doi.org/10.1016/S0065-2776(08)00001-1

Grönholm, M., F. Jahan, S. Marchesan, U. Karvonen, M. Aatonen, S. Narumanchi, and C.G. Gahmberg. 2011. TCR-induced activation of LFA-1 involves signaling through Tiam1. *J. Immunol.* 187:3613–3619. http://dx.doi.org/10.4049/jimmunol.1100704

Harriague, J., and G. Bismuth. 2002. Imaging antigen-induced PI3K activation in T cells. *Nat. Immunol.* 3:1090–1096. http://dx.doi.org/10.1038/ni847

Holt, K.H., L. Olson, W.S. Moye-Rowley, and J.E. Pessin. 1994. Phosphatidylinositol 3-kinase activation is mediated by high-affinity interactions between distinct domains within the p110 and p85 subunits. *Mol. Cell. Biol.* 14:42–49.

Huppa, J.B., M. Gleimer, C. Sumen, and M.M. Davis. 2003. Continuous T cell receptor signaling required for synapse maintenance and full effector potential. *Nat. Immunol.* 4:749–755. http://dx.doi.org/10.1038/ni951

Huse, M. 2012. Microtubule-organizing center polarity and the immunological synapse: protein kinase C and beyond. *Front Immunol.* 3:235. http://dx.doi.org/10.3389/fimmu.2012.00235

Iijima, M., and P. Devreotes. 2002. Tumor suppressor PTEN mediates sensing of chemoattractant gradients. *Cell.* 109:599–610. http://dx.doi.org/10.1016/S0092-8674(02)00745-6

Jaffe, A.B., and A. Hall. 2005. Rho GTPases: biochemistry and biology. *Annu. Rev. Cell Dev. Biol.* 21:247–269. http://dx.doi.org/10.1146/annurev.cellbio.21.020604.150721

Jimenez, C., C. Hernandez, B. Pimentel, and A.C. Carrera. 2002. The p85 regulatory subunit controls sequential activation of phosphoinositide 3-kinase by Tyr kinases and Ras. *J. Biol. Chem.* 277:41556–41562. http://dx.doi.org/10.1074/jbc.M205893200

Kavran, J.M., D.E. Klein, A. Lee, M. Falasca, S.J. Isakoff, E.Y. Skolnik, and M.A. Lemmon. 1998. Specificity and promiscuity in phosphoinositide binding by pleckstrin homology domains. *J. Biol. Chem.* 273:30497–30508. http://dx.doi.org/10.1074/jbc.273.46.30497

Ku, G.M., D. Yablonski, E. Manser, L. Lim, and A. Weiss. 2001. A PAK1-PIX-PKL complex is activated by the T-cell receptor independent of Nck, Slp-76 and LAT. *EMBO J.* 20:457–465. http://dx.doi.org/10.1093/emboj/20.3.457

Leon, J., I. Guerrero, and A. Pellicer. 1987. Differential expression of the ras gene family in mice. *Mol. Cell. Biol.* 7:1535–1540.

Liu, X., J.L. Karnell, B. Yin, R. Zhang, J. Zhang, P. Li, Y. Choi, J.S. Maltzman, W.S. Pear, C.H. Bassing, and L.A. Turka. 2010. Distinct roles for PTEN in prevention of T cell lymphoma and autoimmunity in mice. *J. Clin. Invest.* 120:2497–2507. http://dx.doi.org/10.1172/JCI42382

Loeser, S., K. Loser, M.S. Bijker, M. Rangachari, S.H. van der Burg, T. Wada, S. Beissert, C.J. Melief, and J.M. Penninger. 2007. Spontaneous tumor rejection by *cbl-b*-deficient $CD8^+$ T cells. *J. Exp. Med.* 204:879–891. http://dx.doi.org/10.1084/jem.20061699

Ludford-Menting, M.J., J. Oliaro, F. Sacirbegovic, E.T. Cheah, N. Pedersen, S.J. Thomas, A. Pasam, R. Iazzolino, L.E. Dow, N.J. Waterhouse, et al. 2005. A network of PDZ-containing proteins regulates T cell polarity and morphology during migration and immunological synapse formation. *Immunity.* 22:737–748. http://dx.doi.org/10.1016/j.immuni.2005.04.009

Markiewicz, M.A., L.N. Carayannopoulos, O.V. Naidenko, K. Matsui, W.R. Burack, E.L. Wise, D.H. Fremont, P.M. Allen, W.M. Yokoyama, M. Colonna, and A.S. Shaw. 2005. Costimulation through NKG2D enhances murine CD8+ CTL function: similarities and differences between NKG2D and CD28 costimulation. *J. Immunol.* 175:2825–2833.

Miletic, A.V., D.B. Graham, K. Sakata-Sogawa, M. Hiroshima, M.J. Hamann, S. Cemerski, T. Kloeppel, D.D. Billadeau, O. Kanagawa, M. Tokunaga, and W. Swat. 2009. Vav links the T cell antigen receptor to the actin cytoskeleton and T cell activation independently of intrinsic Guanine nucleotide exchange activity. *PLoS ONE.* 4:e6599. http://dx.doi.org/10.1371/journal.pone.0006599

Mor, A., and M.R. Philips. 2006. Compartmentalized Ras/MAPK signaling. *Annu. Rev. Immunol.* 24:771–800. http://dx.doi.org/10.1146/annurev.immunol.24.021605.090723

Mor, A., G. Campi, G. Du, Y. Zheng, D.A. Foster, M.L. Dustin, and M.R. Philips. 2007. The lymphocyte function-associated antigen-1 receptor costimulates plasma membrane Ras via phospholipase D2. *Nat. Cell Biol.* 9:713–719. http://dx.doi.org/10.1038/ncb1592

Nguyen, K., N.R. Sylvain, and S.C. Bunnell. 2008. T cell costimulation via the integrin VLA-4 inhibits the actin-dependent centralization of signaling microclusters containing the adaptor SLP-76. *Immunity.* 28:810–821. http://dx.doi.org/10.1016/j.immuni.2008.04.019

Nishikimi, A., H. Fukuhara, W. Su, T. Hongu, S. Takasuga, H. Mihara, Q. Cao, F. Sanematsu, M. Kanai, H. Hasegawa, et al. 2009. Sequential regulation

of DOCK2 dynamics by two phospholipids during neutrophil chemotaxis. *Science*. 324:384–387. http://dx.doi.org/10.1126/science.1170179

Nishimura, T., T. Yamaguchi, K. Kato, M. Yoshizawa, Y. Nabeshima, S. Ohno, M. Hoshino, and K. Kaibuchi. 2005. PAR-6-PAR-3 mediates Cdc42-induced Rac activation through the Rac GEFs STEF/Tiam1. *Nat. Cell Biol.* 7:270–277. http://dx.doi.org/10.1038/ncb1227

Nolz, J.C., T.S. Gomez, P. Zhu, S. Li, R.B. Medeiros, Y. Shimizu, J.K. Burkhardt, B.D. Freedman, and D.D. Billadeau. 2006. The WAVE2 complex regulates actin cytoskeletal reorganization and CRAC-mediated calcium entry during T cell activation. *Curr. Biol.* 16:24–34. http://dx.doi.org/10.1016/j.cub.2005.11.036

Nombela-Arrieta, C., R.A. Lacalle, M.C. Montoya, Y. Kunisaki, D. Megías, M. Marqués, A.C. Carrera, S. Mañes, Y. Fukui, C. Martínez-A, and J.V. Stein. 2004. Differential requirements for DOCK2 and phosphoinositide-3-kinase gamma during T and B lymphocyte homing. *Immunity*. 21: 429–441. http://dx.doi.org/10.1016/j.immuni.2004.07.012

Pagès, F., M. Ragueneau, R. Rottapel, A. Truneh, J. Nunes, J. Imbert, and D. Olive. 1994. Binding of phosphatidylinositol-3-OH kinase to CD28 is required for T-cell signalling. *Nature*. 369:327–329. http://dx.doi.org/10.1038/369327a0

Perez de Castro, I., T.G. Bivona, M.R. Philips, and A. Pellicer. 2004. Ras activation in Jurkat T cells following low-grade stimulation of the T-cell receptor is specific to N-Ras and occurs only on the Golgi apparatus. *Mol. Cell. Biol.* 24:3485–3496. http://dx.doi.org/10.1128/MCB.24.8.3485-3496.2004

Purbhoo, M.A., D.J. Irvine, J.B. Huppa, and M.M. Davis. 2004. T cell killing does not require the formation of a stable mature immunological synapse. *Nat. Immunol.* 5:524–530. http://dx.doi.org/10.1038/ni1058

Quann, E.J., E. Merino, T. Furuta, and M. Huse. 2009. Localized diacylglycerol drives the polarization of the microtubule-organizing center in T cells. *Nat. Immunol.* 10:627–635. http://dx.doi.org/10.1038/ni.1734

Rameh, L.E., Ak. Arvidsson, K.L. Carraway III, A.D. Couvillon, G. Rathbun, A. Crompton, B. VanRenterghem, M.P. Czech, K.S. Ravichandran, S.J. Burakoff, et al. 1997. A comparative analysis of the phosphoinositide binding specificity of pleckstrin homology domains. *J. Biol. Chem.* 272:22059–22066. http://dx.doi.org/10.1074/jbc.272.35.22059

Riese, M.J., L.C. Wang, E.K. Moon, R.P. Joshi, A. Ranganathan, C.H. June, G.A. Koretzky, and S.M. Albelda. 2013. Enhanced effector responses in activated CD8+ T cells deficient in diacylglycerol kinases. *Cancer Res.* 73:3566–3577. http://dx.doi.org/10.1158/0008-5472.CAN-12-3874

Robertson, L.K., L.R. Mireau, and H.L. Ostergaard. 2005. A role for phosphatidylinositol 3-kinase in TCR-stimulated ERK activation leading to paxillin phosphorylation and CTL degranulation. *J. Immunol.* 175:8138–8145.

Rodriguez-Viciana, P., P.H. Warne, R. Dhand, B. Vanhaesebroeck, I. Gout, M.J. Fry, M.D. Waterfield, and J. Downward. 1994. Phosphatidylinositol-3-OH kinase as a direct target of Ras. *Nature*. 370:527–532. http://dx.doi.org/10.1038/370527a0

Rodriguez-Viciana, P., P.H. Warne, B. Vanhaesebroeck, M.D. Waterfield, and J. Downward. 1996. Activation of phosphoinositide 3-kinase by interaction with Ras and by point mutation. *EMBO J.* 15:2442–2451.

Sadelain, M., I. Rivière, and R. Brentjens. 2003. Targeting tumours with genetically enhanced T lymphocytes. *Nat. Rev. Cancer.* 3:35–45. http://dx.doi.org/10.1038/nrc971

Sanui, T., A. Inayoshi, M. Noda, E. Iwata, M. Oike, T. Sasazuki, and Y. Fukui. 2003. DOCK2 is essential for antigen-induced translocation of TCR and lipid rafts, but not PKC-theta and LFA-1, in T cells. *Immunity*. 19:119–129. http://dx.doi.org/10.1016/S1074-7613(03)00169-9

Sauer, S., L. Bruno, A. Hertweck, D. Finlay, M. Leleu, M. Spivakov, Z.A. Knight, B.S. Cobb, D. Cantrell, E. O'Connor, et al. 2008. T cell receptor signaling controls Foxp3 expression via PI3K, Akt, and mTOR. *Proc. Natl. Acad. Sci. USA*. 105:7797–7802. http://dx.doi.org/10.1073/pnas.0800928105

Shim, E.K., C.S. Moon, G.Y. Lee, Y.J. Ha, S.K. Chae, and J.R. Lee. 2004. Association of the Src homology 2 domain-containing leukocyte phosphoprotein of 76 kD (SLP-76) with the p85 subunit of phosphoinositide 3-kinase. *FEBS Lett.* 575:35–40. http://dx.doi.org/10.1016/j.febslet.2004.07.090

Shim, E.K., S.H. Jung, and J.R. Lee. 2011. Role of two adaptor molecules SLP-76 and LAT in the PI3K signaling pathway in activated T cells. *J. Immunol.* 186:2926–2935. http://dx.doi.org/10.4049/jimmunol.1001785

Sims, T.N., T.J. Soos, H.S. Xenias, B. Dubin-Thaler, J.M. Hofman, J.C. Waite, T.O. Cameron, V.K. Thomas, R. Varma, C.H. Wiggins, et al. 2007. Opposing effects of PKCtheta and WASp on symmetry breaking and relocation of the immunological synapse. *Cell*. 129:773–785. http://dx.doi.org/10.1016/j.cell.2007.03.037

Somersalo, K., N. Anikeeva, T.N. Sims, V.K. Thomas, R.K. Strong, T. Spies, T. Lebedeva, Y. Sykulev, and M.L. Dustin. 2004. Cytotoxic T lymphocytes form an antigen-independent ring junction. *J. Clin. Invest.* 113:49–57.

Stinchcombe, J.C., and G.M. Griffiths. 2007. Secretory mechanisms in cell-mediated cytotoxicity. *Annu. Rev. Cell Dev. Biol.* 23:495–517. http://dx.doi.org/10.1146/annurev.cellbio.23.090506.123521

Stinchcombe, J.C., E. Majorovits, G. Bossi, S. Fuller, and G.M. Griffiths. 2006. Centrosome polarization delivers secretory granules to the immunological synapse. *Nature*. 443:462–465. http://dx.doi.org/10.1038/nature05071

Stromnes, I.M., J.N. Blattman, X. Tan, S. Jeevanjee, H. Gu, and P.D. Greenberg. 2010. Abrogating Cbl-b in effector CD8(+) T cells improves the efficacy of adoptive therapy of leukemia in mice. *J. Clin. Invest.* 120:3722–3734. http://dx.doi.org/10.1172/JCI41991

Tarasenko, T., H.K. Kole, A.W. Chi, M.M. Mentink-Kane, T.A. Wynn, and S. Bolland. 2007. T cell-specific deletion of the inositol phosphatase SHIP reveals its role in regulating Th1/Th2 and cytotoxic responses. *Proc. Natl. Acad. Sci. USA*. 104:11382–11387. http://dx.doi.org/10.1073/pnas.0704853104

Tybulewicz, V.L. 2005. Vav-family proteins in T-cell signalling. *Curr. Opin. Immunol.* 17:267–274. http://dx.doi.org/10.1016/j.coi.2005.04.003

Vardhana, S., K. Choudhuri, R. Varma, and M.L. Dustin. 2010. Essential role of ubiquitin and TSG101 protein in formation and function of the central supramolecular activation cluster. *Immunity*. 32:531–540. http://dx.doi.org/10.1016/j.immuni.2010.04.005

Varma, R., G. Campi, T. Yokosuka, T. Saito, and M.L. Dustin. 2006. T cell receptor-proximal signals are sustained in peripheral microclusters and terminated in the central supramolecular activation cluster. *Immunity*. 25:117–127. http://dx.doi.org/10.1016/j.immuni.2006.04.010

Wang, F., P. Herzmark, O.D. Weiner, S. Srinivasan, G. Servant, and H.R. Bourne. 2002. Lipid products of PI(3)Ks maintain persistent cell polarity and directed motility in neutrophils. *Nat. Cell Biol.* 4:513–518. http://dx.doi.org/10.1038/ncb810

Yi, J., X.S. Wu, T. Crites, and J.A. Hammer III. 2012. Actin retrograde flow and actomyosin II arc contraction drive receptor cluster dynamics at the immunological synapse in Jurkat T cells. *Mol. Biol. Cell*. 23:834–852. http://dx.doi.org/10.1091/mbc.E11-08-0731

Yokosuka, T., K. Sakata-Sogawa, W. Kobayashi, M. Hiroshima, A. Hashimoto-Tane, M. Tokunaga, M.L. Dustin, and T. Saito. 2005. Newly generated T cell receptor microclusters initiate and sustain T cell activation by recruitment of Zap70 and SLP-76. *Nat. Immunol.* 6:1253–1262. http://dx.doi.org/10.1038/ni1272

Zhang, W., J. Sloan-Lancaster, J. Kitchen, R.P. Trible, and L.E. Samelson. 1998. LAT: the ZAP-70 tyrosine kinase substrate that links T cell receptor to cellular activation. *Cell*. 92:83–92. http://dx.doi.org/10.1016/S0092-8674(00)80901-0

Zipfel, P.A., S.C. Bunnell, D.S. Witherow, J.J. Gu, E.M. Chislock, C. Ring, and A.M. Pendergast. 2006. Role for the Abi/wave protein complex in T cell receptor-mediated proliferation and cytoskeletal remodeling. *Curr. Biol.* 16:35–46. http://dx.doi.org/10.1016/j.cub.2005.12.024